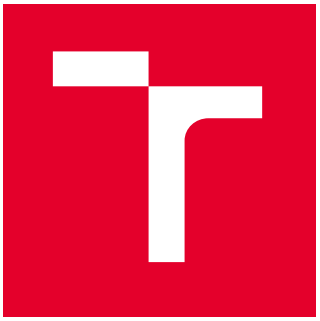

BRNO UNIVERSITY OF TECHNOLOGY

VYSOKÉ UČENÍ TECHNICKÉ V BRNĚ

FACULTY OF MECHANICAL ENGINEERING

FAKULTA STROJNÍHO INŽENÝRSTVÍ

INSTITUTE OF PROCESS ENGINEERING

ÚSTAV PROCESNÍHO INŽENÝRSTVÍ

FLOW OF COMBUSTION AIR IN THE BURNER OF A ROTARY KILN

PROUDĚNÍ SPALOVACÍHO VZDUCHU V HOŘÁKU ROTAČNÍ PECE

MASTER'S THESIS

DIPLOMOVÁ PRÁCE

AUTHOR — **Bc. Michal Dorniak**

AUTOR PRÁCE

SUPERVISOR — **Ing. Jiří Vondál, Ph.D.**

VEDOUCÍ PRÁCE

BRNO 2023

BRNO UNIVERSITY OF TECHNOLOGY
FACULTY OF MECHANICAL ENGINEERING

Assignment Master's Thesis

Institut:	Institute of Process Engineering
Student:	**Bc. Michal Dorniak**
Degree programm:	Process Engineering
Branch:	no specialisation
Supervisor:	**Ing. Jiří Vondál, Ph.D.**
Academic year:	2022/23

As provided for by the Act No. 111/98 Coll. on higher education institutions and the BUT Study and Examination Regulations, the director of the Institute hereby assigns the following topic of Master's Thesis:

Flow of combustion air in the burner of a rotary kiln

Recommended bibliography:

BAUKAL, Charles E. Computational Fluid Dynamics in Industrial Combustion. Boca Raton: CRC Press, 2001. ISBN 0-8493-2000-3.

ARIYARATNE, W.K. Hiromi, Anjana MALAGALAGE, Morten C. MELAAEN a Lars-andré TOKHEIM. CFD modelling of meat and bone meal combustion in a cement rotary kiln – Investigation of fuel particle size and fuel feeding position impacts. Chemical engineering science [online]. Elsevier, 2015, 123, 596-608 [cit. 2022-10-20]. ISSN 0009-2509. Dostupné z: doi:10.1016/j.ces.2014.10.048

MIKULČIĆ, Hrvoje, Damijan CERINSKI, Jakov BALETA a Xuebin WANG. Improving Pulverized Coal and Biomass Co□Combustion in a Cement Rotary Kiln by Computational Fluid Dynamics. Chemical engineering & technology [online]. Frankfurt: Wiley Subscription Services, 2019, 42(12), 2539-2545 [cit. 2022-10-20]. ISSN 0930-7516. Dostupné z: doi:10.1002/ceat.201900086

Deadline for submission Master's Thesis is given by the Schedule of the Academic year 2022/23

In Brno,

L. S.

prof. Ing. Petr Stehlík, CSc., dr. h. c. Director of the Institute	doc. Ing. Jiří Hlinka, Ph.D. FME dean

ABSTRACT

The presented master's thesis focuses on the computational fluid dynamics (CFD) simulation of combustion air within a cement rotary kiln burner and the area immediately behind the burner. The research was conducted in collaboration with the cement plant Českomoravský cement, a.s., facility location Mokrá. The initial sections of the thesis provide an overview of the current state of cement production. The subsequent part discusses the principles and calculations involved in CFD simulations, along with other important parameters necessary for a comprehensive and accurate presentation of the obtained results. The second part of the thesis focuses on the development and meshing of the burner model. Data for creating the model were collected during multiple visits to the cement plant, where real measurements of the burner were conducted.

The simulations in this study aimed to comprehensively analyse the detailed behaviour of combustion air. Through these simulations, several areas requiring optimization were identified and subsequently improved. An additional simulation was conducted to evaluate the optimized state. Another significant aspect considered in this thesis is the erosion assessment of the pulverized coal channel. Multiple simulations were performed to determine the areas most affected by erosion. In the final section of the thesis, various approaches to address this issue are suggested.

Keywords

CFD simulation, multichannel rotary kiln burner, combustion airflow, primary air, erosion by coal particles

ROZŠÍRENÝ ABSTRAKT

Predložená diplomová práca sa vo svojej väčšej časti zaoberá CFD simuláciami. Cieľom tejto práce bolo komplexne zmapovať správanie sa prúdenia spaľovacieho vzduchu v horáku rotačenej pece a jeho bezprostredne nadväzujúcej oblasti. Celý proces vypracovania tejto diplomovej práce prebiehal v spolupráci s cementárňou Českomoravský cement, a.s., lokácia Mokrá, ktorá slúžila ako primárny zdroj údajov a validácie výsledkov. Každá CFD simulácia potrebuje pre jej úspešné overenie porovnanie s experimentálnymi dátami, čo sa nám základe spolupráce podarilo splniť.

V úvodných častiach práce bol popísaný proces výroby cementu a používaná technológia práve v cementárni Českomoravský cement, a.s., prevádzka Mokrá. Následne boli popísané základné teoretické a výpočtové princípy CFD analýz s doplnením popisu doležitých parametrov potrebných na posúdenie výsledkov. Kontkrétna príprava na simuláciu prebiehala najskôr prvotným meraním skutočného horáku rotačnej pece priamo v cementárni. Takéto merania sa uskutočnili dve, pretože cementáreň disponuje dvomi rôznymi pecnými linkami. Používané horáky v jednotlivých linkách sa trochu odlišujú vo svojej najpodstatnejšej časti, v špičke horáku. Cieľ práce bol zamerať sa na horák s modernejším usporiadaním pre maximalizáciu prínosu zistení do budúcnosti.

Prvé meranie sa uskutočnilo na horáku so staršou konfiguráciou, pretože pre nás podstatný, modernejší horák bol v tej dobe stále v prevádzke. Na základe prvého merania spolu s dostupnou a vzhľadom na vek neúplnovou výkresovou dokumentáciou, bol vytvorený model pomocou programu SolidWorks. Po neskoršom druhom meraní bol tento model prakticky overený a následne upravený, aby odpovedal modernejšej verzii horáku. Skúsenými inžinieromi zvalidovaný model, slúžil ako základ pre následujúcu prípravu celej simulácie. Príprava simulácie pozostávala z tvorby optimálnej siete, ktorá tvorila približne 60 % náročnosti úspešného vykonania analýzy a vhodným nastavením použitých výpočtových metód.

Vykonané simulácie boli zamerané na dva väčšie ciele. Najkôr bolo vyhodnodnotené správanie spaľovacieho vzduchu v horáku a tesne za ním. Odhalené nedostatky boli s cementárňou prediskutované a boli navrhnuté možné riešenia problému. Druhým cieľom bolo vyhodnotenie erózneho poškodenia uhoľného kanálu. Poškodenie uhoľného kanálu bol odpozorované pri pravidelných údržbách horáku.

Pre všetky zistené nedostatky boli navrhnuté možnosti, kde by sa práca mohla do budúcnosti pokračovať. Pre prípad spaľovacieho vzduchu bol optimalizovaný stav aj simulovaný.

KĽÚČOVÉ SLOVÁ

CFD simulácia, viackanálový horák rotačnej pece, prúdenie spaľovacieho vzduchu, primárny vzduch, erózia časticami uhlia

BIBLIOGRAPHIC CITATION

Printed version:

DORNIAK, Michal. *Flow of combustion air in the burner of a rotary kiln*. Brno, 2023. Available at: https://www.vut.cz/studenti/zav-prace/detail/150628. Master's thesis. Brno University of Technology, Faculty of Mechanical Engineering, Institute of Process Engineering. Thesis supervisor Jiří Vondál.

Online version:

DORNIAK, Michal. *Flow of combustion air in the burner of a rotary kiln* [online]. Brno, 2023 [cit. 2023-05-22]. Available at: https://www.vut.cz/studenti/zav-prace/detail/150628. Master's thesis. Brno University of Technology, Faculty of Mechanical Engineering, Institute of Process Engineering. Thesis supervisor Jiří Vondál.

SIGNED DECLARATION

I, Michal Dorniak, hereby declare that this thesis entitled "*Flow of combustion air in the burner of a rotary kiln"* is a product of my original work and was composed by myself under the supervision of Ing. Jiří Vondál, Ph.D. All literature used in the research and creation of this work has been properly referenced.

In Brno 26/05/2023 ……..

Michal Dorniak

WORD OF ACKNOWLEDGEMENT

I would like to express my sincere gratitude and appreciation to my supervisor, Ing. Jiří Vondál, Ph.D, for his invaluable guidance, support, and expert advice throughout the journey of completing my master's thesis. I am grateful for his continuous encouragement, patience, and availability whenever I sought clarification or faced challenges. His profound knowledge and expertise in the field have greatly enriched my understanding and helped shape the quality of my work.

Furthermore, I would like to extend my sincere thanks to cement plant Českomoravský cement a.s., location Mokrá for their collaboration and support in the creation of this master's thesis. Their contribution and cooperation have been crucial in acquiring the necessary data and insights for the successful completion of this research.

I would also like to express my appreciation to the staff of the Institute of Process Engineering at the Faculty of Mechanical Engineering who have contributed to my academic journey. The choice of the Institute of Process Engineering as the institution for pursuing my master's degree has been one of the best decisions I have made, and I am incredibly proud to be a part of such a prestigious institute.

Contents

1 Introduction

The cement manufacturing process involves a highly complex and energy-intensive series of chemical and physical transformations that take place inside a rotary kiln. The efficiency of this process is strongly influenced by the performance of the rotary kiln burner, which is responsible for introducing the fuels and combustion air into the kiln. However, the design and operation of the rotary kiln burner is a challenging task due to the complex interactions between the combustion air (primary air), secondary air and diverse range of fuels employed, which can result in uneven temperature distributions, poor combustion efficiency, and high wear rates in critical components.

To address these challenges, this master thesis aims to map in detail the behaviour of combustion air in the burner of a cement rotary kiln and immediately after it, using advanced computational fluid dynamics (CFD) modelling tools. Specifically, the study will determine the pressure drops for individual combustion air branches, which is critical for optimizing mass flow distribution and combustion efficiency. Furthermore, erosion-stressed coal feed points will be identified, and modifications proposed to reduce wear rates in these critical components.

Overall, the aim of this study was to contribute to the field of cement manufacturing, to provide insights into the operation of the rotary kiln burner and the potential to improve the performance and efficiency of the entire combustion process. The findings of this investigation are intended to be beneficial to professionals in the cement industry, as well as researchers and engineers, and should establish a solid foundation for future research endeavours in this field.

1.1 Cement production technology

This research was conducted in a mutually cooperative manner with a cement production facility Českomoravský cement a.s., location Mokrá. As such, the forthcoming section shall provide a concise exposition of the technology and procedures employed within the factory, followed by a more in-depth examination of the combustion process and the associated technology, which are of utmost relevance to the objectives of this thesis. Figure 1 presents a comprehensive depiction of the entire cement production process.

The technology of cement production at the Českomoravský cement, a.s., facility location Mokrá, starts with the extraction of limestone and corrective shale in a quarry two kilometres away from the plant. The extraction of these raw materials is carried out by quarry blasting. Wheel loaders and large tonnage trucks are used to transport and load raw materials from the individual mining areas to the crushing facility. The current mining area is 120 ha with an approximate annual production of 1 500 000 tonnes [1]. The raw material is crushed in two hammer crushers and transported by conveyor belts to the raw material hall at the plant for further processing in the production technology.

The pre-crushed raw material and the requisite correction component are conveyed from the raw material hall to the raw material mills, where it is subjected to grinding and drying processes. The homogenized raw material is then put into storage silos for later usage.

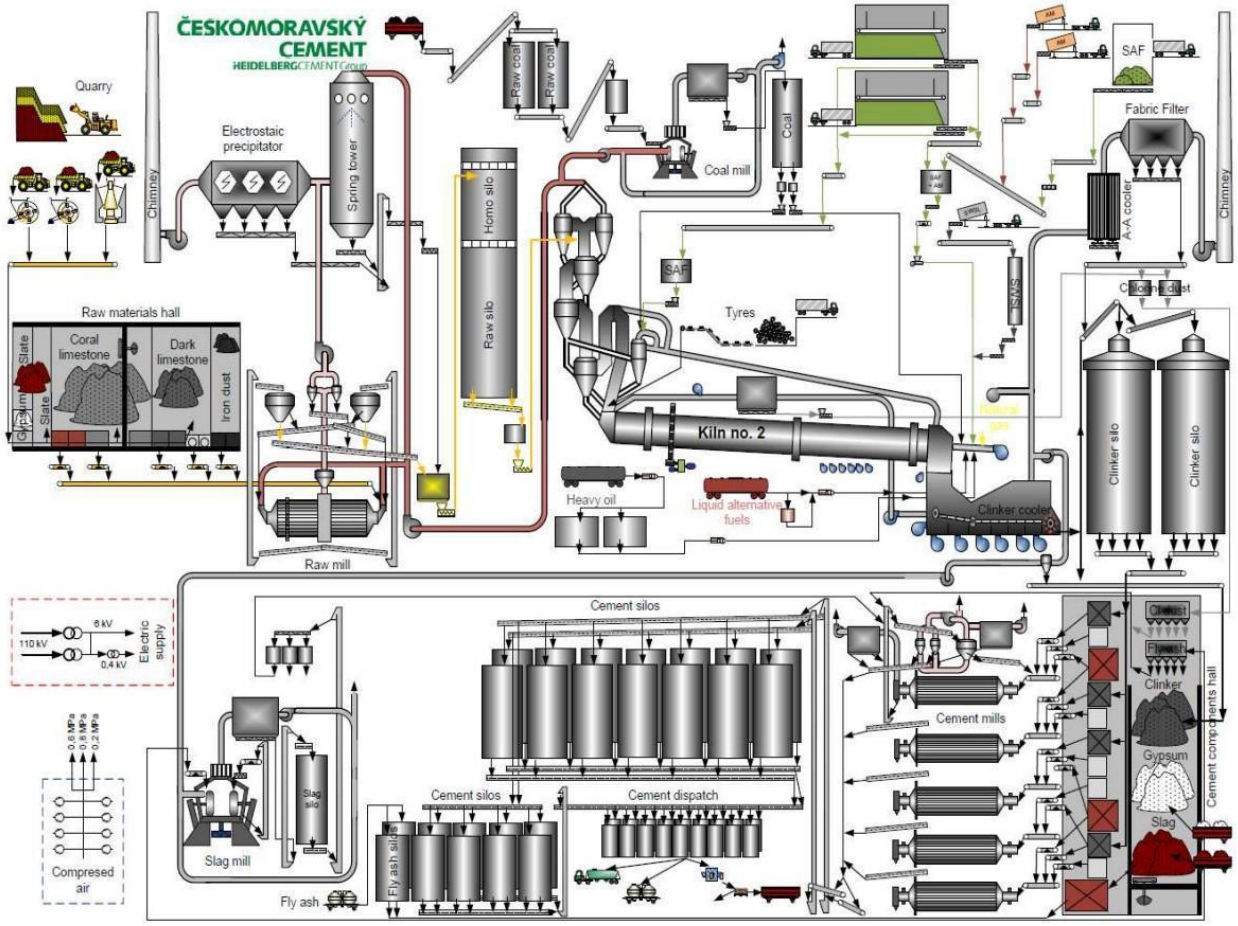

Fig. 1 *Schematic diagram of cement production facility Českomoravský cement, a.s., location Mokrá [1]*

The raw material is at this point ready for the production's most crucial task - clinker formation.

The process begins in the preheater tower, where the raw meal is preheated by transferring the heat from the hot exhaust gases to the incoming raw meal. The tower is made up of cyclones connected by vertical conduits. The raw meal is introduced into the vertical shaft where it is entrained in the gas exiting the cyclone below. This is the stage where the heat transfer takes place. The exhaust gases exit the cyclone from the top, while the raw meal, which is heated, drops to the cyclone below. This entire process is then repeated.

After the preheating, the process moves to the subsequent stage in the furnace line. The enlonged calcination channel and calcination chamber (secondary combustion chamber) located at the bottom of the preheater tower, which have been explicitly engineered for the combustion of alternative fuels. Here, the limestone in the raw meal is thermally broken down. Fuel and tertiary air, from the grate cooler, are injected into a riser duct which causes limestone to oxidize, turning it into lime. Currently, the pre-calciner runs at temperatures over 800 °C [2].

The next unit is the rotary kiln, with a diameter of 4,3 x 67 meters, which is the primary combustion chamber [1]. The raw meal is introduced into the kiln's higher end, and as the raw meal moves along the length of the kiln, it is exposed to temperatures ranging from 1,400 °C to 1,450 °C, depending on the process requirements [12].

Within the kiln, various physical and chemical reactions occur between the raw meal, which leads to the formation of clinker minerals. The materials' size and composition, as well as the residence time in the kiln, determine the final clinker's properties.

Once the clinker has been formed, it is then rapidly cooled in a grate cooler, which is the final unit of the combustion process. The cooler's primary purpose is to stabilize the clinker, reduce its temperature, and prevent undesirable reactions from taking place.

The described combustion process is shown in the following figure.

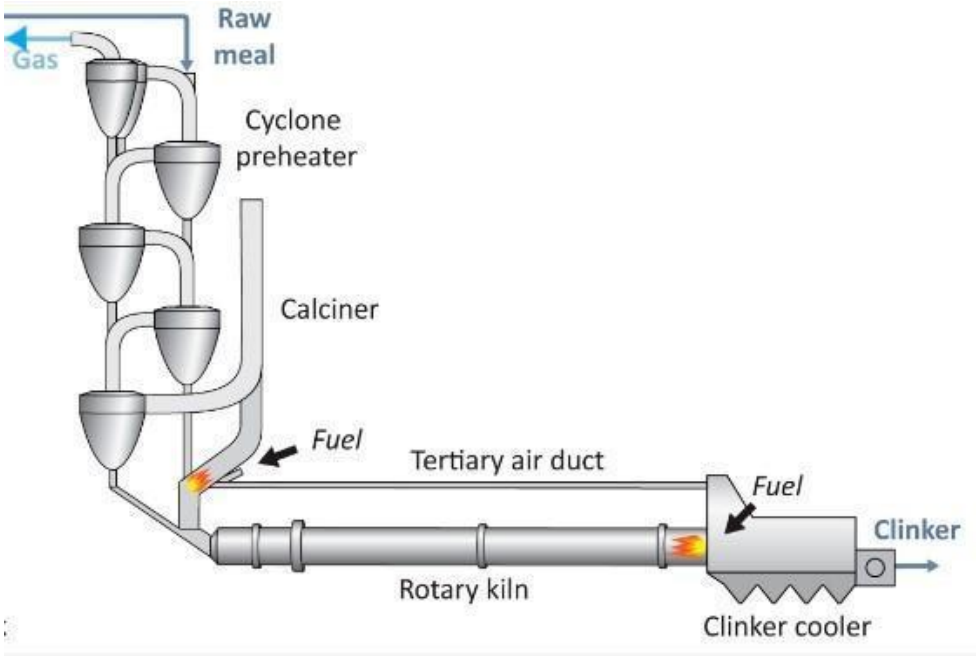

Fig. 2 *The furnace line of clinker production [3]*

Afterwards, the clinker is crushed into small particles measuring 5-10 mm in size before being stored in clinker silos [4]. This crushing process is carried out using cone or rebound crushers. Afterwards, the clinker is transported to the ball mills along with additives such as gypsum, where it is ground to the necessary fineness. The resulting cement, which meets the required quality standards, is then transported either pneumatically or mechanically to reinforced concrete silos. Finally, the cement is prepared for onward shipment.

1.2 Combustion process

Combustion is one of the most important processes in engineering, which involves turbulent fluid flow, heat transfer, chemical reaction, radiative heat transfer and other complicated physical and chemical processes. Typical engineering applications include internal combustion engines, power station combustors, furnaces, as well as cement rotary kiln burners. It is important to be able to predict the flow, temperatures, resulting species concentrations and emissions from various combustion systems for the design and improvement of combustion equipment, particularly with the current concerns about CO2 and other emission levels and their effects on the environment. The emissions of greenhouse gases caused by cement production are distributed in the following way: calcination accounts for 50 %, fuel consumption for 40 %, while the remaining 10 % comes from indirect emissions caused by vehicular traffic and electricity production [2]. The emissions are related to the manufacturing of clinker, which is

done at temperatures above 1,400 °C [5]. It all comes down to the combustion process, therefore the understanding and accurate prediction of flow patterns become even more critical in the cement industry.

As the traditional techniques are either difficult, expensive or impossible to describe the flow patterns, CFD modelling comes into play. CFD modelling of combustion systems proves to be beneficial to understand the fluid flow, fuel combustion and heat transfer phenomena in rotary kilns. More detailed insights into CFD modelling are described in a separate chapter.

Traditional combustion may be represented symbolically as follow:

Fig. 3 *Combustion scheme*

As the figure suggests the type of fuels used has a big impact on the entire cement production process, especially combustion. The following section will examine and provide a description of the various fuel types used.

1.2.1 Coal

Coal is a fundamental fossil fuel consisting of carbon-rich solid material that can serve as an energy source. There are several varieties of coal, categorized based on their carbon content. In cement production, different types of coal are utilized, including anthracite, bituminous coal, and lignite, which may vary by region and availability, with bituminous coal being the most prevalent choice. [6]

Typically, coal with a volatile content ranging from 18 % to 22 % is utilized in cement production [8]. If required, a suitable blend of high-volatile coal (gas coal or fat coal) and low-volatile coal (lean coal or anthracite) can be utilized as a fuel source.

Coal is a secure and safe fuel source, as it poses no significant risks during transportation, storage, and utilization. However, the combustion of fossil fuels, like coal, emits significant amounts of carbon dioxide into the atmosphere, contributing significantly to global warming. Despite its substantial environmental impact, coal combustion remains the primary energy source for cement plants worldwide, accounting for 90 % of their energy consumption [7]. The abundance and ease of extraction of coal compared to other fossil fuels have traditionally made it the preferred fuel source in the cement industry. Nevertheless, in recent years, there has been a growing emphasis on alternative fuels due to environmental concerns regarding greenhouse gas emissions (particularly CO2) and waste management issues, resulting in a reduction in coal usage.

1.2.2 Natural Gas

Natural gas is currently the most frequently used of gaseous fuels, those that naturally exist in a gaseous state under normal temperature and pressure. It is a fossil fuel made of hydrocarbons

that were transformed over millions of years by pressure and temperature acting on plant and animal wastes that were buried beneath many layers of rock and soil. In cement plants, natural gas is the most common form of gaseous fuel and is typically transported to the plant through pipelines under high pressure. However, the gas must be depressurized to 3-10 bar before it can be utilized [12]. Gas is frequently used to heat kilns since it is simple to ignite.

The use of natural gas as fuel has a number of significant benefits:

- **Higher heating value** - Natural gas outperforms all other fossil fuels in terms of heating value per mass unit with an average value of 38.58 MJ/Nm^3 [9].
- **Cleanest fuel** - Since it is primarily composed of methane (according to [9] - 95.52 %), its combustion produces water and carbon dioxide, which are also gases exhaled by living things when they breathe.
- **Lesser "greenhouse effect" -** When compared to fuel oil and coal, natural gas combustion results in 31 % and 38 % less CO2 emissions, respectively, while delivering the same amount of energy [9].

The following table provides general information about of natural gas supplied by a certain Canadian distributor.

Tab. 1 *Combustion characteristics of Natural Gas [9]*

Ignition point	590 °C to 650 °C
Flammability limits (% volume of air)	4.3 % to 15 %
Theoretical flame temperature	1940 °C
Maximum flame velocity in air	0.30 m/s

1.2.3 Petcoke

Petcoke is a byproduct of oil refining obtained from the thermal breakdown of heavy oils. It primarily comprises carbon, although it may also contain substantial amounts of sulfur and heavy metals. In simple terms, the use of petcoke as a fuel in cement plants has been popularized over the last decade as it is considered "the cheapest unit of energy" without compromising the quality of the final product. This has led to petcoke becoming one of the most commonly used fuels in cement kilns globally, as the cost per unit of released energy during firing is usually cheaper compared to coal and fuel oil. [9]

To use petcoke as a fuel in cement kilns, it must be pulverized and burned in the main burner or even in the secondary combustion chamber. The main challenge of using petcoke as a fuel is its low volatile content, which affects flame control [9]. Petcoke flames are typically longer than those produced by oil or coal, which negatively impacts the production process in cement kilns. This longer flame can result in poor granular conditions and the formation of larger crystals, which can impact both the energy consumption for milling and the strength characteristics of the resulting cement. Therefore, controlling the ignition of petcoke is essential to achieving optimal flame shape in cement kilns.

1.2.4 Oil

Usually, rotary kilns are powered by heavy fuel oil, known as fuel oil. The fuel oil used should have low sulfur content or a more expensive low-sulfur oil (fuel oil E1) should be used. The oil is viscous at low temperatures and must be heated to about 50 °C for tank discharge, pumping, and handling. To achieve good atomization in burners, the oil temperature must be further increased to 120 °C, which is done using a special oil as a heat transfer medium (thermal oil). Fuel oil pumping pressures range from 40 to 60 bar, with maximum flow velocities of about 0.2 m/sec on the suction side and 0.4 m/sec on the delivery side of pumps. To achieve optimal firing conditions, the pressure and temperature of the oil supplied to the burners should be ideally constant. [8]

To conclude this section on conventional fuels used in the cement industry, Table 2 has been provided to compare the cost per fuel unit. Together with the information provided in each section regarding a particular fuel, it should now be clear what strengths and weaknesses the various fuels possess.

***Tab. 2** Comparative cost of the energy unit for various fuels [9]*

Fuel	Comparative Cost
Petcoke	30 up to 50
Coal	100
Oil	150 up to 250
Gas	200 up to 300

1.2.5 Alternative fuels

Cement manufacturers worldwide are looking to cut their production costs, and using alternative fuels is an effective way to achieve this goal. The use of low-grade alternative fuels like waste coal, tyres, sewage sludge, and biomass fuels (such as wood products, agricultural waste, etc.) in pre-calciner vessels is a viable option because the combustion temperature is lower. Precalciner vessels are equipped to reduce NOx emissions due to reburn reactions when kiln exhaust gases pass through them. When waste is combusted in cement kiln systems instead of dedicated incinerators, there is a net global reduction in CO2 emissions, resulting in a reduction in CO2 penalties. Alternative fuels are often cheaper than conventional fossil fuels, providing the possibility of a competitive advantage. [10]

1.3 Industrial rotary kiln burners

One of the most crucial components of a rotary kiln is the burner since it controls the airflow field, temperature distribution, energy use, consumption of refractory clay bricks, and even the lifespan of the kiln. Figure 3 shows the evolution of rotary kiln burners in the cement industry. Further specification of such burners is described in the following section.

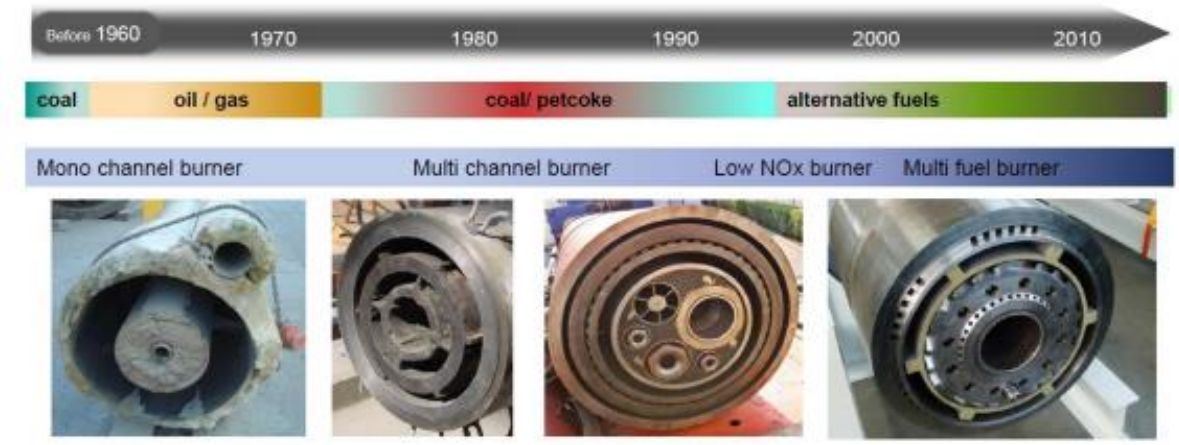

Fig. 4 *Development of the cement burner technology [12]*

A burner in a cement kiln together with a calciner can produce between 1000 and 12,000 tons of clinker per day with a thermal capacity of roughly 20 to 250 MW [11].

Single-Channel Burners (Mono-Channel)

The early kiln burners were single-channel burners typically fired with pulverised fuel, i.e. coal. Fuel and primary air are injected through a single channel and outlet velocities of the air are typically 40-60 m/s [12]. They use a high amount of primary air (15-45 %) to ensure a high burner momentum [12]. A higher momentum gives a more efficient mixing of air and fuel in the kiln and thus promotes proper combustion of fuel.

Aside from the high amount of primary air, the disadvantages of single-channel burners include the inability to change the load (limited turndown ratio), making them difficult to manage during start-up operations. Furthermore, because the amount of primary air and coal throughput must be proportionate, changing the flame pattern during operation is extremely limited. Control can be gained by adjusting the primary air velocity and amount, based on the fuel load. [17]

This type of burner is suitable for long kilns of wet and semi-wet cement production without separate calcination and preheating.

Low Primary Air Burners (low NO_X burners)

Low NO_X burners were developed in the 1980s in response to stricter environmental regulations. NO_X formation increases with increasing temperature and oxygen availability, so the principles for reducing NO_X involve stabilising the flame and recirculating combusted gases, concentrating the fuel along the centre axis to prevent it from leaving the flame, and reducing the amount of primary air to 8-10 % (compared to 10-15 % in a multichannel burner). [14]

NO_X is mainly formed if the fuel is allowed to burn in oxygen-rich conditions. Thus, low NO_X burners use a low amount of primary air, typically less than 10 %. This decreases the availability of oxygen in the hot part of the flames and lowers the production of NO_X. [12]

The low NO_X burners are typically not suitable for high utilisation of alternative fuels due to the insufficient primary air and burner momentum, which makes it difficult to ignite the alternative fuel particles and can lead to unburnt fuel particle dropout [12].

Multichannel Burners

An example of a modern multichannel burner is shown in Fig 5.

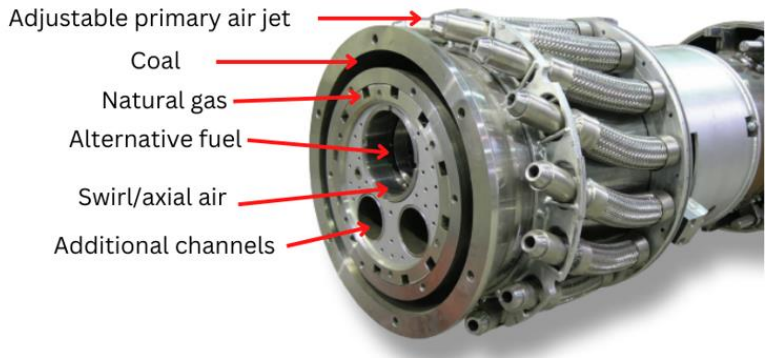

Fig. 5 *M.A.S kiln burner [13]*

Most modern cement kiln burners are so-called multichannel burners, which contain several channels and nozzles for the injection of different kinds of fuel and air. Different tubes and annular channels are applied with the possibility of burning both pulverised and lumpy solid fuels as well as liquids and gases.

One of the main factors that differentiate commercial burners is the primary air injection. In modern rotary kiln burners, it is becoming common to use primary air jets, either adjustable or fixed, to create a low-pressure zone between the jets which draws in hot secondary air for increased mixing and faster ignition of the fuel.

The burner shown in Fig. 5 is designed with adjustable primary air hoses. By adjusting the angles of these hoses, we are capable of bringing the whole primary air into a swirling flow, thus they are used to shape the flame. The central tube for solid alternative fuels may be equipped with an additional pneumatic injector system (as in our case). This system would be responsible for accelerating the alternative fuel velocity and creating a swirling flow to distribute the fuel in the flame zone.

A swirl/axial air expands the flow of pulverised fuel and stabilises the flame by creating an internal recirculation zone (shown in Fig. 6). The high degree of flame shaping is beneficial to adjust a burner to the requirements of each single kiln system. It helps in kiln optimization, securing a stable coating formation, kiln shell temperature, and clinker quality. [17]

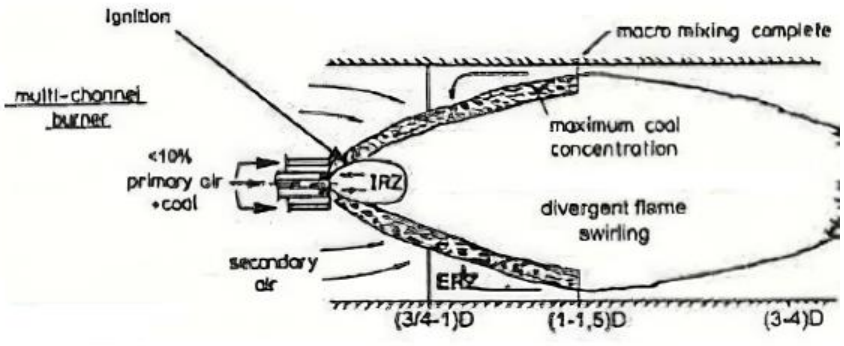

Fig. 6 *Burner coal flame [12]*

1.4 Ideal characteristics of the rotary kiln burner

As mentioned, the purpose of the rotary kiln burner is to produce flame to provide thermal energy to the raw materials enabling a temperature increase from about 900 to 1450 °C [12], to facilitate liquid phase formation and clinkerisation reactions, in the burning zone. The ideal characteristics of the rotary kiln burner are: [12]

- to provide a short, narrow, highly radiant flame to enable efficient heat transfer to the clinker bed,
- to ensure the complete burning of solid fuels while suspended in the flame,
- to produce the minimum of CO and NOx,
- to ensure a stable coating formation in the burning zone,
- to operate with a minimum of primary and transport air,
- to operate with a minimum of excess air, and
- to be able to handle a flexible choice of both conventional fossil fuels and alternative fuels.

The flame properties are of importance for the clinker quality and for the pyro-system stability and efficiency. Inefficient heat transfer to the clinker bed can result in high amounts of free lime in the clinker, hence lower alite (C_3S) content and a lower strength of the cement product. Long, high-temperature flame may cause unwanted crystal growth of the clinker minerals which reduces the clinker grindability and increases the energy consumption for grinding. Too wide a flame can cause impingement on the clinker bed increasing sulphur evaporation and flame impingement on the kiln walls may lead to coating breakdown which may shorten the lifetime of the kiln refractory. [11] Since we know the importance of the shape of the flame, we need to know how to regulate it to our advantage. To do this, we must familiarise ourselves with the different burner designs as each burner has its own ways of regulating the flame.

1.5 Combustion air in a cement kiln burnerto

The oxidizer, in most cases air, is a key component of the combustion process, which has a direct influence on the quality of the product of the process, economic costs, CO2 emissions and so on. In order to control and optimise the combustion, in-depth knowledge of airflow is required. In the following section, the distribution and the purposes of the combustion air in a cement kiln burner are presented.

Fig. 7 illustrates the combustion-air flow and its distribution in a cement kiln burner.

<table>
<tr><td colspan="3">EFFECTIVE COMBUSTION-AIR</td></tr>
<tr><td colspan="2">REQUIRED COMBUSTION-AIR
100%</td><td>EXCESS AIR
10%</td><td rowspan="2">FALSE
AIR 1%</td></tr>
<tr><td>PRIMARY
AIR 12-14%</td><td colspan="2">SECONDARY AIR 96-98%</td></tr>
</table>

***Fig. 7** Typical combustion-air distribution [11]*

Primary air is defined as air passing through the burner. It consists of axial air, radial air and fuel-conveying air. The percentage of primary air in the required combustion air is called the primary air ratio.

A low heat value of fuel increases fuel consumption and the requirement of air for combustion. The effective air for combustion is composed of primary air, hot secondary air from the clinker cooler (supplied through the rotary kiln hood) and false air infiltrating through openings and sealing.

Almost all equipment installed for surveillance or operational purposes gives rise to false air. Primary air should be below and false air completely avoided, from the thermal efficiency point of view. Excess air (above the stoichiometric requirement, expressed as a ratio) is required to ensure complete combustion. A high excess air ratio reduces energy efficiency and the increased exhaust gas amounts may limit the production capacity. [11]

Non-preheated primary air, which makes up about 5-15 % of the required stoichiometric air, is typically sent through the burner pipe at a high velocity of 150-250 m/s. This primary air is often injected both axially and tangentially, with the axial injection providing burner momentum and the tangential injection creating a swirling flow. The remaining combustion air, called secondary air, is supplied through the rotary kiln hood from the clinker cooler, which has a temperature of around 1000 °C. The excess air ratio is typically between 1.10 and 1.25. [11]

2 Burner airflow

The airflow in a cement burner is an important factor in the efficient operation of a cement rotary kiln. It helps to provide the oxygen necessary for the combustion of the fuel, as well as to mix the fuel and combustion air. The airflow is typically controlled by adjusting the size of the burner orifices and the velocity of the primary air. By carefully adjusting these parameters, it is possible to optimise and control the flame in the cement kiln.

The airflow in a cement burner is also influenced by the fuel type and its calorific value, as well as the temperature and composition of the cement being produced in the kiln.

However, there are several key parameters that have to be taken into account when optimising the burner airflow, including the mixing rate of oxygen, which is the major factor for an efficient combustion process. In this section, the theory of the mixing process will be described in further detail.

2.1 Burner momentum

When it comes to primary air, most people think of burner momentum. The burner momentum describes how well the hot secondary air, at about 1000 °C [11], is mixed with the cold (ambient) primary air. Using only 10 % of combustion air, the burner must be able to generate a sufficient entrainment force to quickly mix the 90 % hot secondary air with the fuel [15]. The common rule is that the higher the burner momentum, the better the combustion. Because the faster the secondary air is mixed with the fuel, the faster the fuel will heat up and ignite. In most cases, it is the rate at which oxygen is mixed with the fuel that determines the rate of combustion, rather than the chemical reactions involved in the combustion process [12].

Burner momentum is defined as follows [15]:

$$\frac{mass\ of\ primary\ air\ \cdot\ its\ injection\ speed}{thermal\ capacity\ of\ the\ burner} = specific\ primary\ air\ momentum\ \left[\frac{N}{MW}\right] \quad (1)$$

The burner momentum became more and more important when cement plants were looking for cheaper fuels. First came the use of petcoke, followed by the utilisation of solid secondary fuels. Nowadays the industry is looking at ways to fire 100 % solid secondary fuels.

However, it is only possible to measure the installed primary air momentum and not the effective momentum available for flame shaping. The installed momentum is defined by the primary air fan or blower installed. If the momentum should be increased, the amount or pressure of the primary air has to be increased which leads to higher operational costs [15].

Although, this is not the only option when it comes to the momentum topic. We are also able to optimise the effective momentum by reducing the inner and outer losses of the burner. Modern multichannel burners consist of only one primary air channel and therefore no mixing losses at the burner tip. This means the pressure drop through the burner is decreased. In other words, installing a bigger fan is not necessary to achieve better results. [15]

2.2 Burner tip geometry

As we already know, primary air is the air injected directly into the burner at a low temperature but at high speed. It has two functions:

1. Cooling the burner
2. Activation of combustion and control of the flame shape

To do this, this primary air is injected at the end of the burner, at high pressure (between 100 and 500 mbar) and at high speed (between 80 and 350 m/s) in order to [16]:

- to draw the hot secondary air into the heart of the flame and to ensure its rapid mixing with the fuel of the burner and thus to activate the combustion,
- to control the flame shape by its axial and radial components, such as its width and length.

Using high-pressure, low-temperature primary air can have an impact on the energy balance of the process due to the energy required to pressurise it and the introduction of cold air into the process. To minimise this impact and optimise its use, it is important to have a high expansion speed for the primary air when sucking in secondary air. To achieve this, it is recommended that:

- the pressure before the end of the burner must not be affected by adjusting elements or pressure drop in order to obtain the maximum expansion speed at the end.

There are geometries of the burners which generally consist of two primary air outlets, at least one of which is axial and the other radial (or rotational). In this case, adjusting the proportion between the flow rate and/or the axial and radial air pressure allows adjustment of the overall radial component of the primary air and varies the flame shape [16]. But considering the fact,

these are a bit outdated, it was necessary to come up with modifications that resulted in increased burner efficiency.

The several disadvantages of burners with two primary air outlets are:

For example, the provision of radial air within the fuel system increases the risk of ejection of fuel out of the flame, which can create adverse operating conditions (deterioration of the cooking quality of the product), operating difficulties, reduction of the lifetime of the brickwork lining the furnace ...) and increases the NOx emissions because the concentration of fuel is too low in the centre of the flame which prohibits the phenomenon of NOx-reducing combustion [16]. Therefore, we will concentrate on the rotary kiln burners that have a single primary air outlet with an adjustable radial component, as shown in Figure 5. In that case:

The radial component is obtained by the orientation of the burner outlet sections. This orientation must be done without any particular pressure loss so that the burner has a primary air expansion rate at the optimal nozzle and better energy efficiency [16]. To conclude:

Most up-to-date modifications that resulted in increased burner efficiency [16]**:**

- Application of having just one primary air channel. Hence no mixing losses at the burner tip, which means the pressure drop through the burner was lower than with traditional burners.
- Modification of the internals (especially the nozzle head) – a lower distance of the flexible hoses and nozzles to the burner mouth, wider air nozzle opening, and inclination of the flexible hoses.
- If the burner tip is not designed to minimise pressure drop, the effective momentum will be much lower than expected, downgrading the mix and wasting energy.

Despite these benefits, controlling the flame diameter in burners with a single primary air outlet that has an adjustable radial component is harder compared to burners with two or more outlets. This is because, in burners with two or more outlets, the axial outlet is generally located at the periphery of the burner to control and stabilise the divergence of the flow and allow a more effective and finer adjustment of the flame diameter. However, this benefit is not present in single-outlet burners, making it harder to adjust the diameter. A large flame diameter can have significant impacts on the process conditions (such as the material being cooked and/or the operating conditions) and the lifespan of refractory furnace coatings. [16]

2.3 Jet expansion

Recirculation is a crucial factor in the formation of turbulent diffusion flames in rotary kilns. By the entrainment action of the confined jet, the reactants are mixed with further secondary air and with recirculated combustion products. This enhances mixing and increases the amount of time that particles spend in the reaction zone during pulverised fuel combustion. This improves the efficiency of gas-solid combustion reactions. [19]

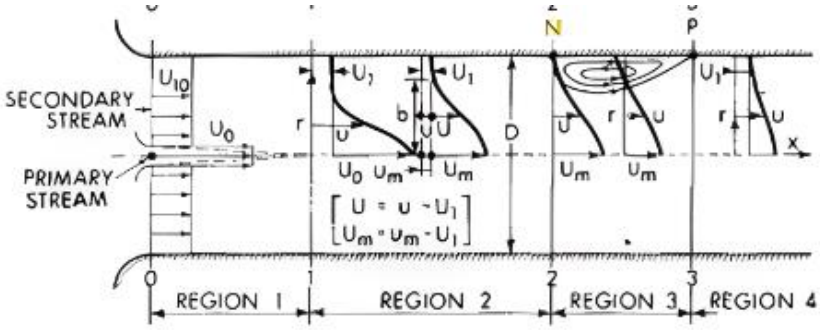

Fig. 8 *Schematic sketch for confined jets - asymmetric case [18]*

Figure 8 is a schematic representation of the flow development of fluid mixing in co-flow. It shows a circular jet issuing axially into a duct with a uniform velocity of U_0. This is generally known as the primary stream. The secondary stream is the surrounding fluid moving in the same direction as the primary stream at the plane of the nozzle with a uniform velocity of U_{10}. As the distance from the nozzle increases, the turbulence generated at the intersurface invades into the primary stream and the potential core of the primary jet is completely consumed at section 1. The distance between the nozzle and section 1 is shown as region 1. Taking the secondary stream into account, it may lose some of its flow to the primary stream due to entrainment. If the ratio U_0/U_{10} is fairly large, it can create an adverse gradient in the axial direction and slow down the secondary stream, causing it to be completely consumed in section 2. Beyond Section 2, with certain flow conditions, a stale eddy or region of recirculation is formed in Region 3. Beyond the end of Region 3, the flow eventually degenerates to a fully developed pipe flow. [18]

2.3.1 Craya-Curtet parameter

In rotary cement kilns, the secondary air is introduced at lower velocities compared to the primary air. This means that the secondary air is introduced as a stream with little momentum and is fully entrained by the primary air jet before any recirculating gas is entrained. Craya and Curtet used this assumption to develop a relation between momentum ratios, known as the Craya-Curtet parameter, using the similarity laws between free and confined jets. [19] The difference between confined and free jets is shown in Figure 9.

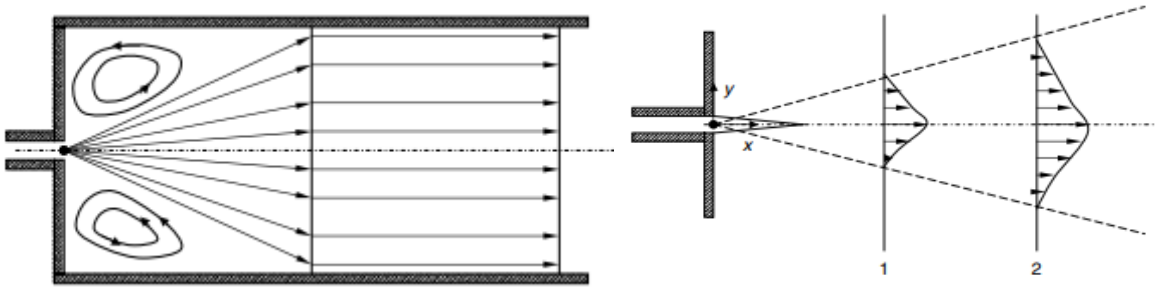

Fig. 9 *Turbulent confined & free jet, respectively [19]*

Craya-Curtet parameter is useful in rotary kilns as a qualitative measure of the extent of recirculation of entrained gases and serves as a way to characterise the shape and intensity of rotary kiln flames without the need for complex CFD calculations.

The Craya-Curtet parameter is defined as follows [19]:

$$M = \frac{3}{2}R^2 + R + \frac{KR^2}{(r_0/L)^2} \quad (2)$$

where R is the discharge ratio, q/Q; $q = (u_0 - u_a)r_0^2$; $Q = u_a(L-\delta^*)^2 + q$, K is a factor relating to the shape of the velocity profile, u_0 is the jet velocity and u_a is the surrounding fluid velocity, δ^* is the boundary layer displacement thickness defined as $1.74/\sqrt{\text{Re}}$; L is the half-width of the combustion chamber (rotary kiln) duct, and r_0 is the radius of the jet nozzle.

The Craya-Curtet parameter is a measure of the aerodynamic mixing between the primary and secondary air streams. It is typically used to classify flames as either short and intense ($M \geq 2$) or long and lazy ($M \leq 1$). Flames with M between 1 and 2 are characterised as long flames with an intensity suitable for processes such as rotary limestone calcination kilns. The parameter is calculated as the ratio of the primary air jet momentum to the secondary air momentum. [19]

2.4 Swirling flows

While the previous analysis only considered axial flow, in cement kiln burners, tangentially injected air, known as swirl air, is used to create a rotating motion that significantly influences the flow field, flame size and stability, and jet expansion. The use of swirl air can significantly improve flame characteristics in cement kilns.

A high swirl number can improve the mixing of the fuel and air, leading to a more stable flame and better heat transfer to the cement. On the other hand, a low swirl number may result in incomplete mixing of the fuel and air, leading to an unstable flame and reduced heat transfer to the cement. In addition, the refractories in the kiln and the burner's wear can both be impacted by the swirl number. The higher intensity of the swirling gas flow that results from a high swirl number might result in increased wear on the refractories and the burner. Therefore, it is important to carefully balance the swirl number to optimise the performance of the rotary kiln while minimising the wear on the burner and refractories.

The swirl number is defined as follows [19]:

$$S = \dot{L_0}/(\dot{G_0}d_0) \quad (3)$$

The nozzle flux of angular momentum $\dot{L_0}$ and the flux of linear momentum $\dot{G_0}$ might be calculated as:

$$\dot{L_0} = 2\pi\rho \int_0^{r_0} (\vec{u}\vec{w})_{nozzle} r^2 dr \quad (4)$$

$$\dot{G_0} = 2\pi \int_0^{r_0} (P + \rho\vec{u})_{nozzle} r dr \quad (5)$$

where d_0 and r_0 are the respective nozzle diameter and radius, and P is the static or gauge pressure P is included to allow for pressure variations due to centrifugal forces. However, the measurements are often difficult or impossible to obtain, therefore the following approximation [19] based on the maximum axial and tangential velocities at the exit of the burner nozzles was proposed.

$$S_g = \frac{r_0 \pi r_e}{A_t} \frac{{Q_\tau}^2}{{Q_T}^2} \tag{6}$$

Where A_t is the total area of the tangential inlets and r_e is the radius at which the tangential inlets of the swirl vanes are joined in relation to the centre axis. The tangential flow rate and total flow rate are denoted by $Q\tau$ and Q_T, respectively. It is discovered that S and S_g are directly proportional [19].

However, for evaluation in the CFD solver, the following formulation is more suitable [39]:

$$\mathrm{S} = \frac{\int_A \rho\, uwr dA}{\mathrm{R} \int_A \rho\, u^2 dA} \tag{7}$$

where u is axial velocity (m/s), w is circumferential velocity (m/s) , ρ is density (kg/m^3), r is radius (m), R is the maximum radius of the nozzle exit (m), A = surface area (m^2).

In order to calculate the swirl number in Fluent, a custom field function had to be created initially. This function evaluated the tangential velocity at a specific radius, as Fluent does not provide this calculation by default. Additionally, a parameter was defined to specify the radius for the swirl number calculation. Once these initial steps were completed, the tangential and axial velocities were evaluated on a designated plane or surface. Having all the necessary components in place, an expression was formulated to describe the swirl number formula, enabling the determination of the swirl number for the selected plane or surface. Afterwards, the process was repeated for a different location in the kiln.

3 Numerical simulations

Although the emphasis of this work is on the combustion airflow in the burner, we still need to understand the detailed processes that take place inside each of the many channels. Every flow occurring inside the kiln burner is a reacting flow type, which is almost always multicomponent, composed of fuel, oxidizer, combustion products, particulates, and so forth. The thermodynamic and transport properties of multicomponent reacting fluids are functions, not only of temperature and pressure but also of species concentration.

It would be possible to get more insight, through mathematical modelling. However, only a few expressions have existed so far. This is caused by the complexity of heat transfer that occurs concurrently with chemical and mineralogical reactions. Furthermore, it is difficult and even impossible to measure the precise physical parameters on-site.

Understanding the fluid flow in such a system by CFD modelling proved to be advantageous. By computationally resolving a set of generalised conservation equations for flow (Navier Stokes equations) and a related set of equations including enthalpy, combustion, and other variables, it is possible to mimic the physical and chemical processes of the reacting flow. The finite-difference or finite-element approximations are key techniques for the numerical simulation of the governing equations. The fundamental equations that describe the simplest case of reacting turbulent flow include conservation equations for mass, concentration, momentum, and enthalpy equations [19].

Continuity Equation:

$$\frac{\partial p}{\partial t} + \frac{\partial}{\partial x_j}(\rho u_j) = 0 \tag{8}$$

Momentum Equation:

$$\frac{\partial}{\partial t}(\rho u_i) + \frac{\partial}{\partial x_j}(\rho u_j u_i) = -\frac{\partial P}{\partial x_i} + \frac{\partial}{\partial x_j}\left[\mu\left(\frac{\partial u_j}{\partial x_i} + \frac{\partial u_i}{\partial x_j}\right)\right] + \rho g_i \tag{9}$$

Concentration Transport Equation:

$$\frac{\partial}{\partial t}(\rho Y_s) + \frac{\partial}{\partial x_j}(\rho u_j Y_s) = \frac{\partial}{\partial x_j}\left(D_\rho \frac{\partial Y_s}{\partial x_j}\right) - w_s \tag{10}$$

Enthalpy Transport Equation:

$$\frac{\partial}{\partial t}(\rho c_p T) + \frac{\partial}{\partial x_j}(\rho u_j c_p T) = \frac{\partial}{\partial x_j}\left(\lambda \frac{\partial T}{\partial x_j}\right) + w_s Q_s \tag{11}$$

Arrhenius Equation:

$$w_s = B\rho^2 Y_F Y_{ox}{}^{-E/RT} \tag{12}$$

Equation of State:

$$P = \rho RT \sum Y_s / M_s \tag{13}$$

This is the system of equations that are used often in CFD codes. However, the most important aspect is the physical interpretation of these complex equations. The engineer can use the similarity parameters derived from these equations to determine which flow characteristics matter the most in the design and operation of the burner. The similarity parameters for the reacting flows can be calculated using the momentum and energy equations as follows [19]:

Euler Number (might be defined as the ratio of the pressure head and the velocity head):

$$Eu = \frac{P_\infty}{p_\infty {U_\infty}^2} \tag{14}$$

Reynolds Number (represents the ratio inertial force and the viscous force):

$$Re = \frac{U_\infty L}{v_\infty} \tag{15}$$

Mach Number (similarity parameter defined as the ratio between kinetic energy and thermal energy):

$$Ma = \sqrt{\frac{{U_\infty}^2/2}{c_p T_\infty}} \approx \frac{U_\infty}{a} \tag{16}$$

Peclet Number (similarity parameter for heat transfer within the fluid defined as the ratio of heat convection and heat conduction):

$$Pe = \frac{U_\infty L}{\lambda_\infty/(c_p p_\infty)} = Re \cdot Pr \tag{17}$$

Damkohler I & Damkohler II (which compare, respectively, the time it will take to the reacting fluid to travel the combustion chamber to the reaction time, and the time it takes the reacting molecules to diffuse to the reaction front and the reaction time).

Damkohler I - (heat of reaction)/(heat of convection) = (flow time)/(reaction time)

$$D_I = \frac{w_{s\infty} Q_s}{\rho_\infty U_\infty c_p / L} = \frac{\tau_f}{\tau_c} \tag{18}$$

Damkohler II – (heat of reaction)/(heat of conduction) = (diffusion time)/(reaction time)

$$D_{II} = \frac{w_{s\infty} Q_s}{\lambda_\infty T_\infty / L^2} = \frac{\tau_d}{\tau_c} \tag{19}$$

3.1 Turbulence modelling

Turbulence modelling is an important aspect of simulating the flow of gases in a cement rotary kiln burner. Turbulence can significantly affect the heat transfer and mixing of gases, as well as the overall performance of the kiln.

There are several approaches to modelling turbulence in a cement rotary kiln burner. As mentioned, the most common approach is to use computational fluid dynamics (CFD) simulations, which involve solving the governing equations of fluid flow using numerical methods. These simulations allow for predicting flow patterns, temperature distributions, and other important parameters in the burner.

Turbulence can be modelled using a number of different methods, for example, the k-epsilon model, the Reynolds stress model (RSM), the eddy dissipation model, Large Eddy Simulation

(LES) and more. Each of the existing models has its own strengths and limitations, and the appropriate model to use will depend on the specific characteristics of the burner and the desired level of accuracy.

It is important to validate the turbulence model against experimental data in order to ensure its accuracy. This can be done by comparing the results of the simulation to measurements taken in a physical test rig or in an operating kiln.

Overall, turbulence modelling is a crucial part of predicting and optimising the performance of a cement rotary kiln burner. In the following section, the most appropriate turbulence models for our particular case will be presented.

3.1.1 k-ε model

According to [19] the k and ε transport equations are presented as follows, respectively.

$$\frac{\partial}{\partial t}(\rho k) + \frac{\partial}{\partial x_i}(\rho k u_i) = \frac{\partial}{\partial x_j}\left[\left(\mu + \frac{\mu_t}{\sigma_k}\right)\frac{\partial k}{\partial x_j}\right] + G - \rho\varepsilon \tag{20}$$

$$\frac{\partial}{\partial t}(\rho \varepsilon) + \frac{\partial}{\partial x_i}(\rho \varepsilon u_i) = \frac{\partial}{\partial x_j}\left[\left(\mu + \frac{\mu_t}{\sigma_\varepsilon}\right)\frac{\partial \varepsilon}{\partial x_j}\right] + C_{1\varepsilon}\frac{\varepsilon}{k} - C_{2\varepsilon}\frac{\varepsilon^2}{k} + S_\varepsilon \tag{21}$$

Where the generation of turbulence denoted by G comprises two terms:

- the generation of turbulence kinetic energy due to the mean velocity gradients, and
- that due to the generation of turbulence kinetic energy due to buoyancy.

S_ε is the turbulence source and $C_{1\varepsilon}$,$C_{2\varepsilon}$ are model constants.

The k-epsilon model is a widely used turbulence model that is based on the conservation of kinetic energy and dissipation rate of turbulence. According to several sources ([19],[20],[21]), the k-epsilon model used to simulate turbulence in cement rotary kilns and burners has proven in recent years to be sufficiently effective, relatively simple to implement while and at the same time providing acceptable results. However, this turbulence model should only be used in a fully developed turbulent mode. When compared to experimental data, the model generates excessively large turbulence length scales near the wall, which slows or even inhibits flow separation. Because the model predicts attached flow in situations where the real flow can already be severely separated, this, in turn, leads to unduly optimistic design decisions [26]. In other words, the k-epsilon model is not valid for predicting laminar-turbulent transitions in wall boundary layers and it is required to use so-called *near-wall treatments*.

3.1.2 RNG k-ε model

In other publications ([22],[23],[27]) RNG k-ε has been used. Using a mathematical technique called renormalization group methods (RNG), the RNG k-ε turbulence model is developed from the instantaneous Navier-Stokes equations. The analytical derivation provides a model with constants that are different from those in the common k-ε model as well as new variables and functions in the transport equations for k and ε. In equations (22) and (23), the transport equations for the RNG k-ε model are provided [22].

$$\frac{\partial}{\partial x_i}(\rho k u_i) = \frac{\partial}{\partial x_j}\left(\alpha_k \mu_{eff} \frac{\partial k}{\partial x_j}\right) + G_k + G_b - \rho\varepsilon \tag{22}$$

$$\frac{\partial}{\partial x_i}(\rho \varepsilon u_i) = \frac{\partial}{\partial x_j}\left(\alpha_\varepsilon \mu_{eff} \frac{\partial \varepsilon}{\partial x_j}\right) + C_1 \frac{\varepsilon}{k}(G_k + C_3 G_b) - C_2 \rho \frac{\varepsilon^2}{k} - R_\varepsilon \tag{23}$$

Where G_k represents the generation of turbulence kinetic energy due to the mean velocity gradients. G_b is the generation of turbulence kinetic energy due to buoyancy. The quantities α_k and α_ε are the inverse effective Prandtl numbers for k and ε, respectively.

3.1.3 k-ω model

Based on Wilcox's investigation [25] another two-equation turbulence model was derived. Transport equations for k and omega have the following formulations, respectively.

$$\frac{\partial k}{\partial t} + \frac{\partial u_j k}{\partial x_j} = \frac{\partial u_i \tau_{ij}}{\partial x_j} - \beta' k\omega + \frac{\partial}{\partial x_j}\left[\left(\upsilon + \sigma' \frac{k}{\omega}\right)\frac{\partial k}{\partial x_j}\right] \tag{24}$$

$$\frac{\partial \omega}{\partial t} + \frac{\partial (u_j \omega)}{\partial x_j} = \frac{\partial u_i \tau_{ij}}{\partial x_j} - \beta\omega^2 + \frac{\sigma_d}{\omega}\frac{\partial k}{\partial x_j}\frac{\partial \omega}{\partial x_j} + \frac{\partial}{\partial x_j}\left[\left(\upsilon + \sigma \frac{k}{\omega}\right)\frac{\partial k\omega}{\partial x_j}\right] \tag{25}$$

Where α, β, β', σ, σ', σ_d are closure coefficients.

The k-omega-based models in the described family of two-equation models provide a superior wall treatment in comparison to the k-epsilon-based models, making them far more adaptable and accurate, especially for non-equilibrium flows. In other words, models for rough wall treatments and the transition between laminar and turbulent flow are compatible with k-omega models.

There are two model variants. The BSL (baseline model) and the SST (Shear Stress Transport) model. The BSL model has been described above and the SST model is a hybrid model that combines the benefits of both k-epsilon and k-omega models, making it suitable for a wider range of flow conditions. The model has been shown to accurately predict flows with strong streamline curvature or swirling flows, which can be a challenge for other turbulence models. The SST k-omega model includes a correction for the near-wall region, which improves the accuracy of predictions in this region. But on the other side, the model is more computationally expensive than the k-epsilon model, which can be a disadvantage for large-scale simulations.

Ultimately, the best turbulence model for a particular cement rotary kiln burner will depend on the specific characteristics of the burner and the desired level of accuracy. It may be necessary to try several different models and compare the results in order to determine the most suitable model for a given application.

Turbulence model selection

Most of the publications mentioned in *Section 3.1* about *turbulence modelling* use the turbulence model from the k-ε family. However, many of these publications focus on gas-solid turbulence flow with chemical reactions inside the rotary kiln, not inside the burner and the

objective of the present thesis is to describe the flow of combustion air inside the burner. Therefore, the SST k-ω model would be the best choice due to its ability to accurately describe the flow near walls. This claim is also supported by [26] as it proposes using the SST model for most industrial applications due to better flexibility and accuracy.

However, it's important to note that the SST k-ω model is a hybrid model that combines the advantages of the k-ε and k-ω models, making it suitable for simulating a wide range of turbulent flows. It is also more complex and computationally expensive than the k-ε models. This is because the SST k-ω model involves solving additional transport equations for turbulence kinetic energy and its dissipation rate, which increases the computational cost of the simulation.

Despite these “disadvantages” of the SST k-ω model, it is still the only reasonable choice to simulate flow in such a large burner (because of the multiple fuel channels/walls inside the burner). In addition, the SST model is more controversial, which provides confidence in its accuracy and reliability in simulating gas flow inside the burner.

3.1.4 Near-wall Treatments

The existence of walls has a notable impact on turbulent flows. The no-slip condition enforced at the wall affects the mean velocity field. Additionally, the presence of the wall affects turbulence in intricate ways. The velocity fluctuations tangential to the wall are reduced by viscous damping in the immediate vicinity, while kinematic blocking decreases normal fluctuations. However, in the outer part of the near-wall region, turbulence is quickly increased by the production of turbulence kinetic energy because of the significant mean velocity gradients. [28]

The accuracy of numerical solutions for wall-bounded turbulent flows depends significantly on near-wall modelling. Successful predictions of wall-bounded turbulent flows rely on an accurate representation of flow in this region. Turbulent core flow models, such as the k-epsilon models, RSM, and LES, are not directly applicable to wall-bounded flows. The Spalart-Allmaras and k-omega models can be used for the entire boundary layer, but proper mesh resolution is necessary for the near-wall region. [28]

Experimental evidence suggests that the near-wall region can be divided into three layers: the viscous sublayer, where the flow is mostly laminar and viscosity dominates momentum and heat or mass transfer, an intermediate region where both molecular viscosity and turbulence are equally important (buffer layer) and an outer fully turbulent layer, where turbulence plays a major role. [28]

Traditionally, two methods are used to model the near-wall region. In the first method, the viscosity-affected inner region is not resolved. Instead, "wall functions" are used as semi-empirical formulas to connect the wall and fully-turbulent regions, removing the need to modify turbulence models to account for wall presence. The second method modifies turbulence models to enable the resolution of the viscosity-affected region with a mesh that extends to the wall. This approach is referred to as "near-wall modelling". [28] Figure 10 provides a graphic representation of these two approaches.

Further details on this topic can be found in the Ansys fluent theory guide [28].

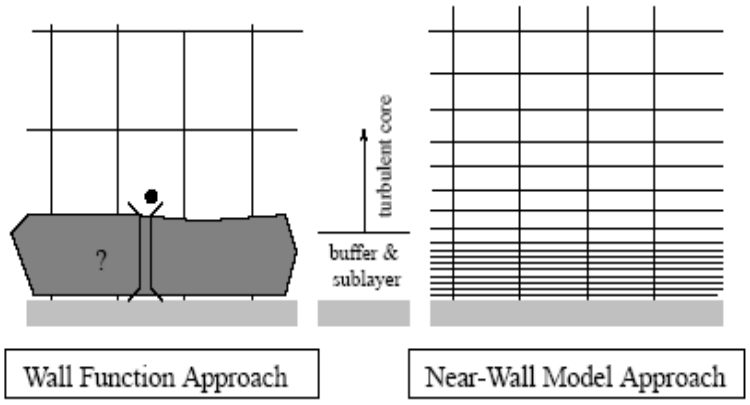

Fig. 10 *Near-wall treatments [28]*

3.2 Particle Modelling

One of the popular methods for simulating the motion and interactions of individual particles in a fluid is the so-called Discrete Particle Model (DPM). In the context of pulverised coal particles, the DPM model can be used to study their behaviour in a flow without considering any chemical reactions (combustion), as in this section of the burner (pulverized coal inlet), the coal particles are only being conveyed by air to the end, where they are ignited. In the following section, we will focus on modelling coal particles and their associated corrections, erosive action, and the calculation of the restitution coefficient.

3.2.1 Discrete Particle Model (DPM)

According to how the fluid and particulate phases are treated, there are three different types of numerical models for particle-fluid flows: Eulerian-Eulerian methods, Lagrangian-Lagrangian methods, and Eulerian-Lagrangian methods. Both the fluid phase and the particle phase are referred to as interpenetrating continuous phases in the Eulerian-Eulerian methods. The Lagrangian frame of reference employs a discrete phase model (DPM) to track particle motion while simultaneously employing an Eulerian formulation for the continuous phase. Many factors (such as viscous drag, lift force, buoyancy, etc.) acting on the Lagrangian particles along their pathways are taken into account, together with the stochastic behaviour of the surrounding turbulent flow. [29]

The trajectory of a discrete phase particle is predicted by integrating the force balance on the particle. This force balance compares the forces exerted on the particle with the inertia of the particle and can be represented as [28]:

$$\frac{du_p}{dt} = F_D\left(u_x - u_{px}\right) + \frac{g_x\left(\rho_p - \rho\right)}{\rho_p} \tag{26}$$

$$F_D = \frac{18\mu C_D Re}{\rho_p {d_p}^2 24} \tag{27}$$

where $F_D\left(u - u_p\right)$ is drag force per unit particles mass, u is the fluid phase velocity, u_p is the particle velocity, μ is the molecular viscosity of the fluid, ρ is the fluid density, ρ_p is the density

of the particle, C_D is the drag coefficient and d_p is the particle diameter. Re is the relative Reynolds number.

The drag coefficient C_D for spherical particles (eq. (28) taken from [30]) and non-spherical particles (eq. (29) taken from [31]) has the following forms, respectively:

$$C_D = a_1 + \frac{a_2}{Re_p} + \frac{a_3}{Re_p} \tag{28}$$

$$C_D = \frac{24}{Re_{sph}}\left(1 + b_1 {Re_{sph}}^{b_2}\right) + \frac{b_3 Re_{sph}}{b_4 + Re_{sph}} \tag{29}$$

where a_1, a_2, a_3 are constants, Re_{sph} is the spherical-particle Reynolds number. b_1, b_2, b_3, b_4 are functions of the sphericity Ø relating the surface area of a sphere having the same volume of the particle and the actual surface area of the particle.

3.2.2 Stochastic particle dispersion modelling

The trajectory of a discrete phase particle relies on knowing the instantaneous local velocity of the gas mixture. To determine this value, the particle motion model can be combined with a stochastic model that considers particle dispersion. *The Random Walk model* is one such model that uses random sampling to determine particle dispersion. Instantaneous flow parameters can be determined by examining a statistically significant number of particle trajectories. These trajectories, which were calculated for various particle sizes and starting points, are often referred to as "tries." Within the chosen model, the instantaneous velocity is calculated as the product of the mean fluid velocity and a random velocity fluctuation with a Gaussian distribution. The fluctuation has a zero mean and a variance that is determined depending on the applied turbulence model and is related to the turbulent velocity scale. [33]

The Rosin-Rammler Distribution

Describing a material composed of multiple-size fractions with a single value parameter is challenging. To accurately represent the size distribution of particles in the system, the Rosin-Rammler mathematical model is employed. This distribution is characterized by several parameters, including *the total flow rate, minimum diameter, maximum diameter, mean diameter, and spread parameter*. These parameters, in addition to the initial velocity, position, and temperature, allow for an efficient representation of the examined sample material.

The mathematical expression of Rosin-Rammler distribution is [38]:

$$F(d) = 100 - 100\exp\left(-\left(\frac{d}{d_0}\right)^m\right), \tag{30}$$

where, under the assumption that all particles have a constant mass density (%), *F(d)* is the mass or volume fraction of particles with sizes lower than or equal to *d* (=undersize distribution). Particle size is given by the parameter *d* (in units of μm), the location parameter d_0 (in units of μm), and the spread parameter *m* of the distribution (m>0).

3.2.3 Erosive action

The erosive impact of particles should not be overlooked as it can result in various issues, including decreased efficiency, heightened maintenance expenses, and safety hazards. To prevent these problems, accurately predicting the trajectories of coal particles is essential.

Accurately predicting the trajectory and behaviour of individual particles in discrete phase simulations heavily relies on how they interact with walls. When a particle comes into contact with a wall, it can experience a range of interactions, such as rebound, sticking, or fragmentation. To account for the interaction between particles and walls in DPM simulations, a variety of models have been developed. These models typically use empirical correlations based on experimental data to predict the outcome of the particle-wall interaction.

Also, it is important to note that the interaction between coal particles (particle-particle interaction) can be neglected because the dispersed phase can exchange momentum, mass, and energy only with the fluid phase [28].

Reflect

As seen in the image below, when a particle hits a boundary, it bounces off the boundary and the momentum of the particle changes according to the restitution coefficient [32]:

$$e_n = \frac{v_{2,n}}{v_{1,n}} \tag{31}$$

where *n* stands for velocity in the normal direction to the wall, *2* represents velocity after the collision and *1* represents velocity before the collision.

The normal coefficient of restitution determines how much momentum is retained by the particle in the direction normal to the wall. The coefficient of restitution for normal or tangential collisions can range from 0 to 1. A restitution coefficient of 1 means that the object maintains its entire momentum after the collision, regardless of direction, which is referred to as an elastic collision. Conversely, if the restitution coefficient is 0, the object loses all of its momentum during the rebound. [32]

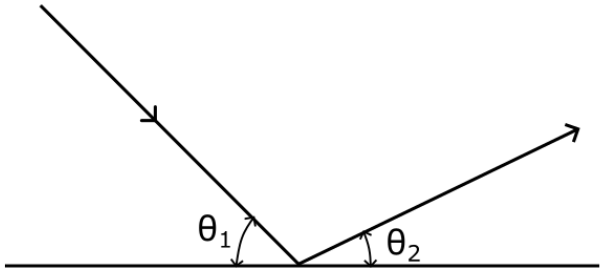

Fig. 11 *"Reflect" Boundary Condition*

Trap

The trajectory calculations are terminated and the condition of the particle is marked as "trapped" (as shown in the figure below). Additionally, a droplet evaporation simulation transforms the entire mass into the vapour phase.

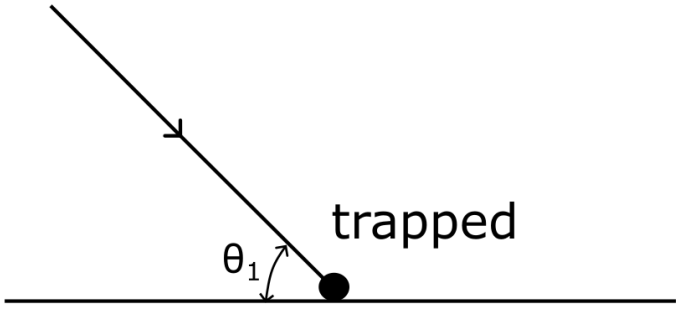

Fig. 12 *Trap Boundary Condition*

Escape

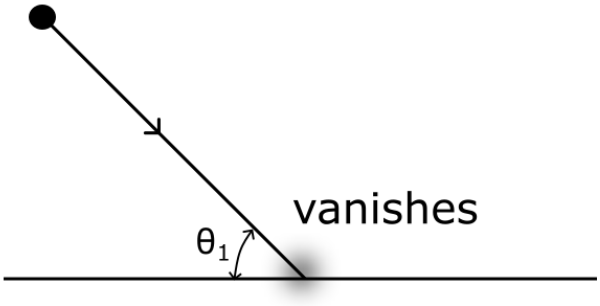

Fig. 13 *Escape Boundary Condition*

When a particle comes into contact with a boundary, it is referred to as "escaped". The trajectory calculations are complete as Figure 13 suggests.

Further details on this topic can be found in the ANSYS FLUENT User's Guide [32].

With the utilisation of previous information, the *erosive wear models* used by Fluent can be introduced. While it is not possible to find a single erosive wear model that can precisely forecast wear in every scenario, the convergence of outcomes from several existing models can offer a more precise and comprehensible understanding of how a broader range of particle sizes affects erosive wear. Previous studies have identified four distinct and widely accepted erosive wear models: *The Generic Model, The Finnie Model, The Oka Model, and The Mclaury Model.* The forthcoming section will include a description of *The Finnie Model*, as this particular model will be employed to assess erosion damage in a rotary kiln burner.

The Finnie Model

The Finnie model was created by Finnie (1960) with the intention of predicting wear generated by particles striking a surface. Equation 31 according to [36] illustrates this model, which uses impact angle and velocity as the underlying variables that affect wear.

$$E = kVf(\gamma) \tag{32}$$

Where E is the mass of eroded material, k is a model constant, V is the velocity of the impacting particle, and $f(\gamma)$ is the following function of the impact angle:

$$f(\gamma) = \begin{cases} \frac{1}{3}\cos^2(\gamma)\,, & 18.5° \leq \gamma \leq 90° \\ sin\,(2\gamma) - 3\sin^2(\gamma)\,, \gamma < 18.5° \end{cases} \tag{33}$$

4 Model Geometry

At the cement plant facility Českomoravský cement, a.s., location Mokrá, two burners are employed. The subsequent images illustrate the primary distinctions between them.

Fig. 14 *Flexible hoses vs Disc design of kiln burner [13]*

One of the burners is operational constantly, while the other is only utilized in specific instances when the primary burner cannot be operated. The significant difference between these burners lies in the crucial part of the burner tip, namely the primary air outlets, which will be the main point of emphasis. The remaining components of the burner tip were previously discussed in *Section 1.3* on *Industrial Rotary Kiln Burners*.

Fig. 15 *Position „0“ (low swirl - long flame) vs Position „10“ (high swirl - short flame) [13]*

The disc technology design is the latest development in optimizing the burner's efficiency. By positioning the adjustable primary air openings directly at the burner tip (Fig. 15), the unobstructed injection of air into the kiln is achieved, compared to the "flexible hoses" design.

This arrangement minimises air losses at the nozzles, resulting in an enhancement of approximately 15 % in the entrainment of secondary air [13].

This year, both burners underwent routine maintenance checks and repairs, presenting an opportunity to conduct measurements. Direct measurements were necessary (Fig. 16) because, over time, some drawings of the burner became unavailable due to its age. Additionally, the burners featured unique modifications that were not documented in the drawings. These modifications were implemented to rectify damages incurred during the operation.

Fig. 16 *Burner parameter recording*

The first complication arose when only the burner with the older design (featuring flexible hoses) was available for measurement, as the other burner was in operation. This thesis aims to provide the most up-to-date insights into the flow of combustion air within the burner, making it preferable to simulate the burner with the latest design, incorporating disc technology. However, considering the limited timeframe for completing this study, it was necessary to measure the burner that was available at that time, in order to initiate the model creation process and potentially create the mesh. Subsequently, once the desired burner (with disc technology) was dismounted for maintenance repairs, the measurements were conducted once again, resulting in adjustments to the model and subsequent recreation of the mesh.

Fig. 17 *Dismounted burner ("flexible hoses design")*

It should be noted that measuring every centimetre of the entire burner was not feasible, hence the done simulation represents the best possible approximation of the combustion airflow within the burner. As an illustration, the internal diameter of one pipe was found to vary at different locations due to in-service damage. Although the difference was insignificant, it was acknowledged and the more conservative option was selected whenever an inconsistency was detected.

Fig. 18 *Burner measurement*

Fig. 19 *Multichannel rotary kiln burner for cement production*

After the initial version of the burner model was established, verification and validation processes were conducted by re-measuring the burner. The updated version was subsequently examined and approved by an experienced cement plant engineer. The final version is shown in Figure 19.

4.1 Created Model

As this study examines the flow of combustion air through multiple channels in a burner, which cannot be adequately expressed by a single image of the model, it is important to provide descriptions and illustrations of these channels, as well as other critical components such as inlets and outlets to facilitate comprehension.

In the given Figure 20, we can observe how the combustion air from the primary air fan is channelled through various cooling channels. These channels serve the primary purpose of maintaining the temperature within the specified range, especially during high-temperature occurrences while operating the burner. Under normal operating conditions, the coal cooling pipe remains closed with a butterfly valve as the air conveying the pulverized coal is sufficient to cool down the channel. Similarly, the flow inside a natural gas cooling pipe is regulated by a butterfly valve, and the same applies to other pipes.

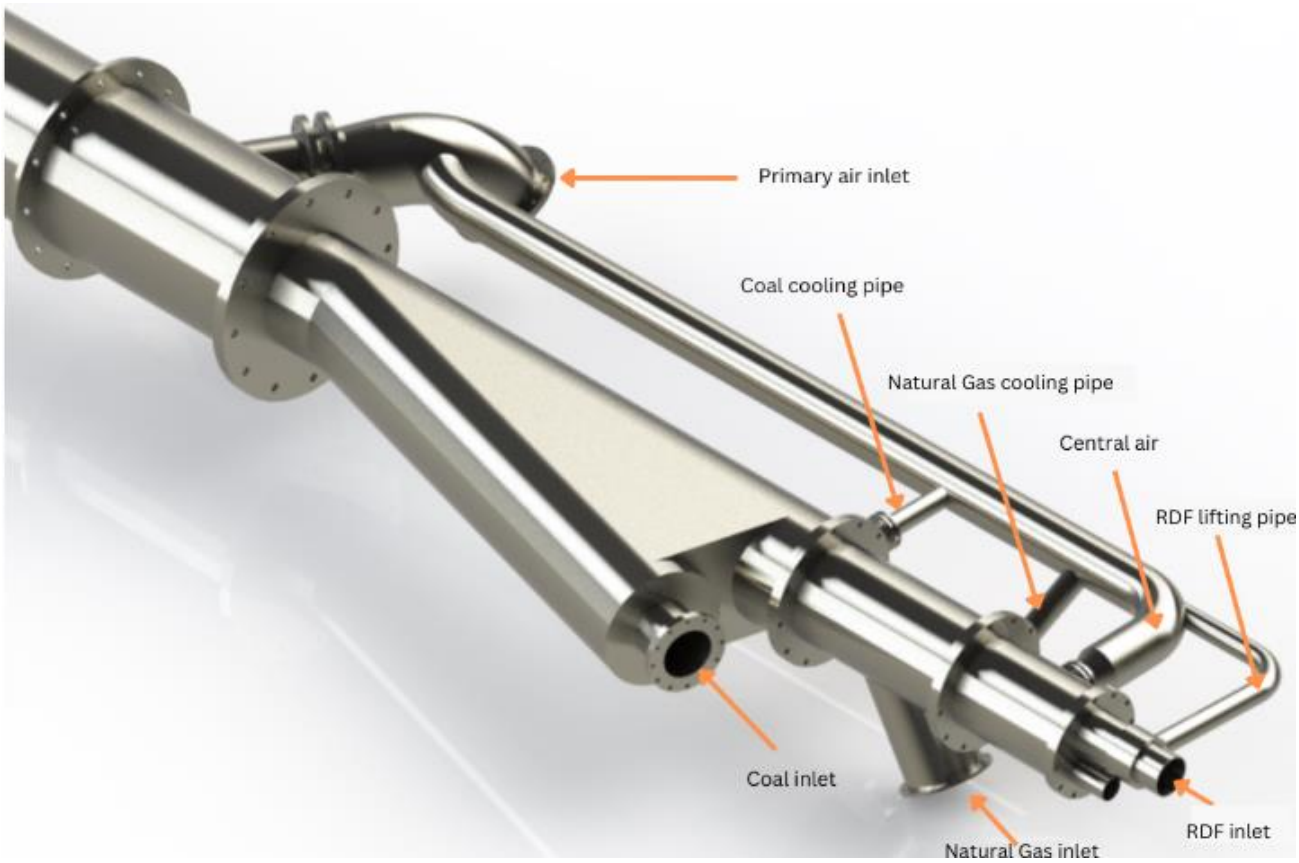

Fig. 20 *Combustion air distribution and fuel inlets*

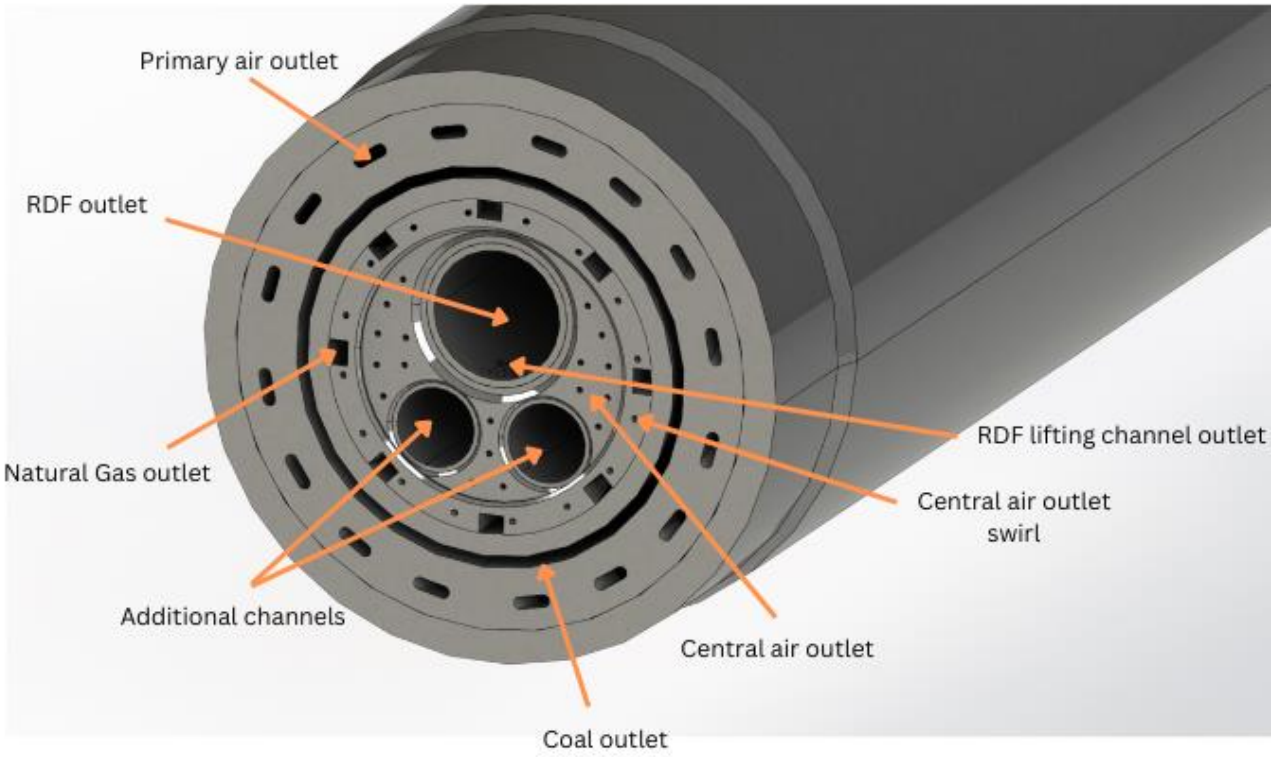

Fig. 21 *Head of the burner - Outlets*

The RDF (Refuse-derived Fuel) lifting pipe, as the name suggests, is responsible for lifting the RDF fuel particles at the end of the RDF channel (close to its outlet) to enhance combustion further in the kiln. Along with the following description of the head of the burner (consisting mainly of various outlets and nozzles), a figure explaining the purpose of the RDF lifting channel is included below. This will help improve understanding.

Fig. 22 *Closer look at the RDF lifting pipe holes*

4.2 Meshing

Computational Fluid Dynamics (CFD) meshing refers to the process of generating a grid or mesh of interconnected elements to represent a physical model in a CFD simulation. The mesh is used to discretise the physical domain into smaller, manageable parts, allowing the simulation to solve the equations that govern fluid flow and heat transfer.

CFD meshing can be performed using various meshing techniques, such as structured meshing, unstructured meshing, and hybrid meshing. Structured meshing generates a grid of uniform elements, while unstructured meshing generates a mesh of elements of varying shapes and sizes to capture complex geometries and flow features better. Hybrid meshing combines the advantages of both structured and unstructured meshing.

The quality of the mesh, in terms of element shape, size, and spacing, is a critical factor in the accuracy and stability of a CFD simulation. To ensure high-quality meshing, various mesh quality metrics are used to evaluate the mesh and identify areas that may require refinement. Commonly used element quality metrics include:

- Aspect Ratio: This measures the ratio of the longest to the shortest edge in an element and is used to determine how well the element is shaped.
- Skewness: This metric measures the deviation of an element from being equilateral and helps to determine the level of element distortion. In other words, skewness refers to the degree of non-uniformity in the cell shape and orientation in a CFD mesh. High skewness can cause issues in the accuracy and convergence of the simulation, so it is desirable to keep the skewness of the mesh low. To achieve this, mesh generation tools often use mesh smoothing techniques to reduce skewness and improve mesh quality.

- Orthogonality: This metric measures the deviation of an element from being orthogonal and helps to determine how well the element is aligned with the flow direction.
- Warpage: This metric measures the deviation of an element from being planar and helps to determine how well the element is suited for representing fluid flow in 3D.

Once the mesh is generated, it can be used to perform CFD simulations by solving the Navier-Stokes equations to calculate fluid velocity, pressure, and temperature, as well as other simulations, such as heat transfer simulations, to analyse and predict fluid behaviour in a given physical system.

In our particular case, the mesh was created using a commercial CFD solver called ANSYS Workbench. We opted to use the "older" approach instead of the Fluent Meshing method due to its superior control and ability to create a highly precise structured mesh. This was absolutely essential for our purposes, given the complexity of the burner and the scope of our investigation.

Initially, the intention was to create a conformal mesh due to its numerous benefits, including flow continuity, accuracy, improved solution convergence, and more. However, it quickly became apparent during the meshing process that this approach would not be feasible. The number of elements was increasing dramatically to the point where it would surpass the capacity of our available computational resources, making it impractical to continue with a conformal mesh.

The subsequent attempt involved dividing the intricate geometry of the burner into smaller, less complex sections. Considering the distinct characteristics of each section, it was apparent that they needed to be treated separately. The sizing requirements for a channel with a width of 10 mm would differ significantly from those of a channel with a width of 50 mm. Furthermore, intersections, inlets, and outlets demanded a much finer mesh due to the complex flow behaviour occurring in these regions. In contrast, areas where the flow exhibited less variation allowed for the use of a slightly coarser mesh.

One such example is the long fuel channels, where the so-called *multizone method* was employed. This method enabled the utilization of hexahedral elements throughout the entire channel, effectively reducing the number of elements required to achieve an acceptable mesh resolution. The image below illustrates one of the many instances where the multizone method was employed, specifically showcasing the part of the mesh within the coal channel.

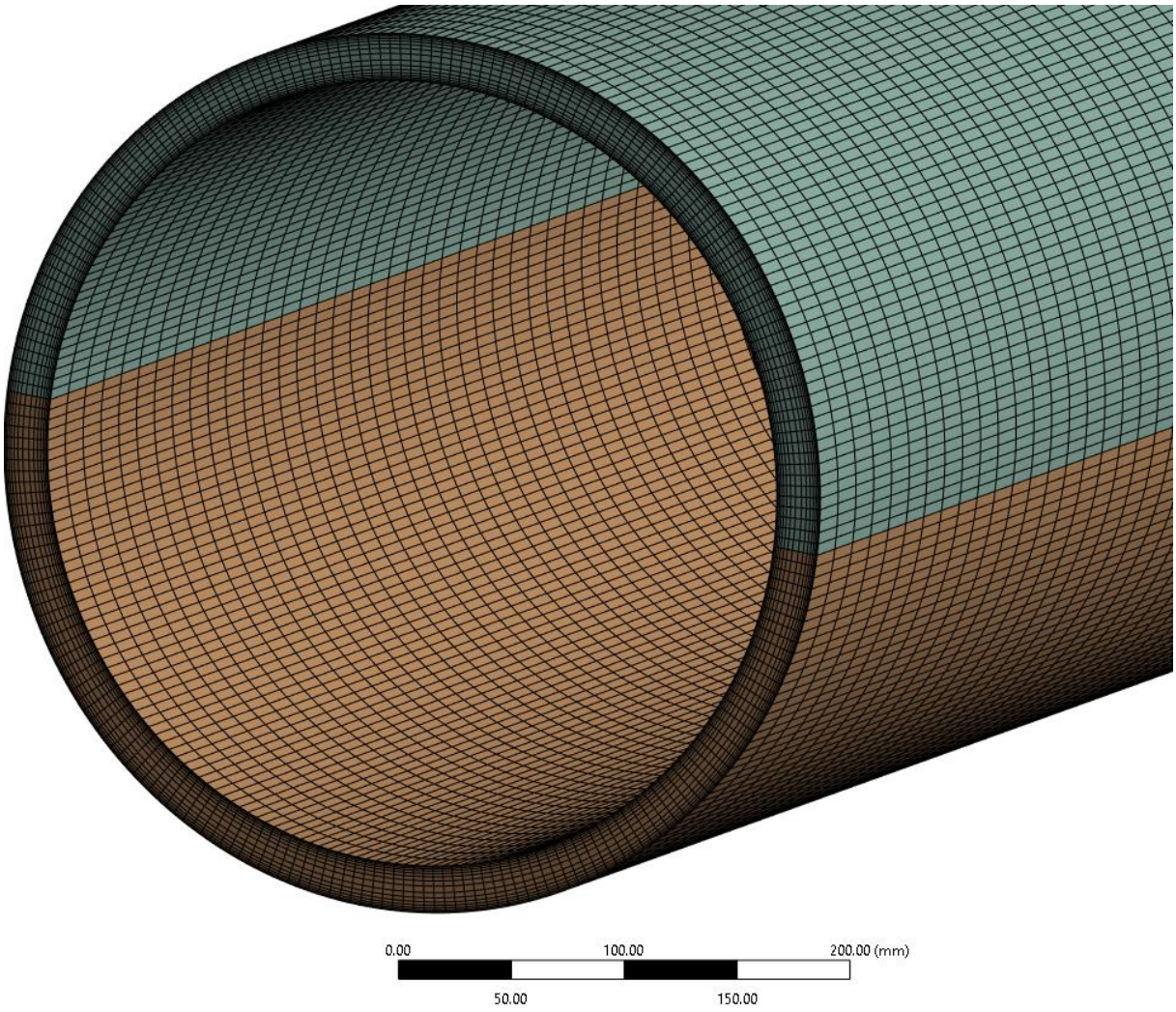

Fig. 23 *Hexahedral mesh of the coal channel*

However, there remained a considerable number of areas where this approach was not applicable, thus demanding the adoption of an unstructured mesh. Nonetheless, the primary objective was to minimize the reliance on an unstructured mesh and restrict its utilization to only those areas where no other viable solution was available.

An example highlighting this can be observed in Figure 24, which illustrates the burner head. In this specific instance, a hybrid mesh was employed. As the name suggests, this mesh comprises both structured and unstructured elements. It is crucial to note that when using this approach, connecting the two types of meshes becomes a critical consideration. Failing to establish proper connections between them can lead to completely erroneous or potentially incomplete solutions. In Fluent, the connection of meshes is achieved by creating interfaces at locations where the meshes differ.

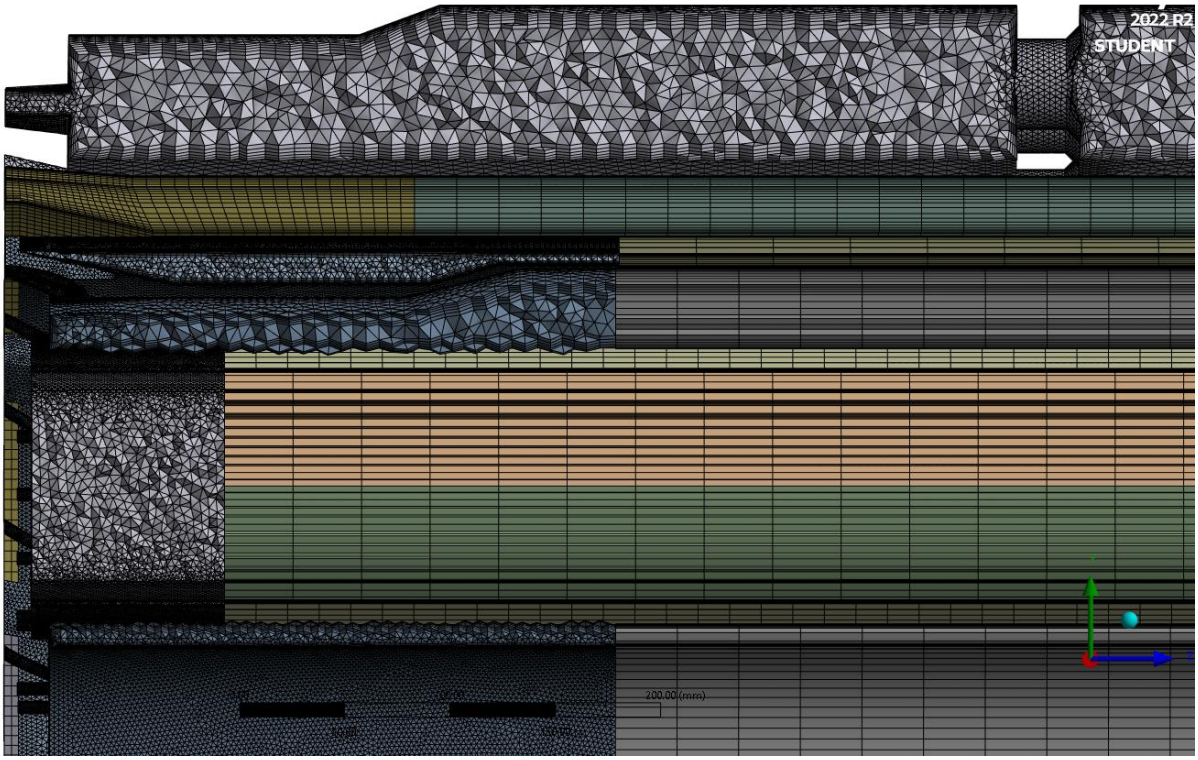

Fig. 24 *Hybrid mesh of the burner's head*

The final constructed mesh consists of approximately *25 million elements*. And although the number of elements is enormous, it is worth noting that this number has already undergone a significant reduction.

In addition to the methods mentioned earlier for element reduction, simplification of the geometry was also necessary. This involved removing certain design elements and negligible parts.

Another contributing factor to the relatively high element count is the inclusion of boundary layers to accurately capture the flow of combustion air near the walls in each channel. These boundary layers are essential for successfully describing and simulating the airflow dynamics in the system.

4.3 Mesh quality

The mesh quality of the analysed model was assessed based on the values of orthogonal quality and skewness. Ideally, a high-quality mesh should have low skewness (0) and high orthogonality (1). The findings revealed an *average value of orthogonal quality of 0,85 and a skewness value of 0,15*. These values are within the acceptable range, indicating that the mesh quality is appropriate for the intended analysis.

It is important to note that to ensure the validity of results, it is essential to conduct a *mesh study* and validate that the numerical solutions are independent of the mesh size. While increasing the number of elements by a factor of two can significantly enhance the accuracy of the model, it comes at the cost of increased computational time and resources.

The created mesh already contains almost 25 million elements. Thus, increasing the mesh size would demand extraordinary computational resources and a corresponding amount of time to

perform a complete and accurate simulation. Instead, the focus was on creating a fine mesh where it is most important, such as at the head of the burner (Fig. 24). This component is critical as it significantly affects both the flame shape and the overall process efficiency.

The following picture visualises the mesh quality (dependence of the number of elements in [%] on skewness).

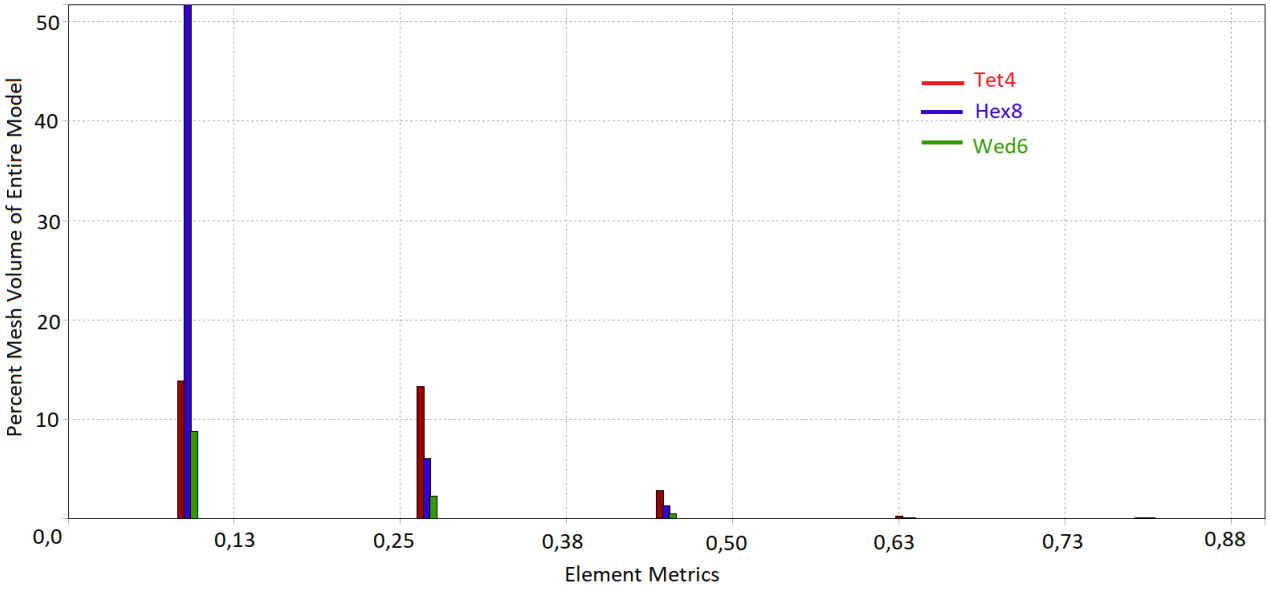

Fig. 25 *Dependence of the number of elements [%] on skewness*

5 Boundary conditions

Simulation setup for combustion air distribution

To summarise the simulation setup, we utilised the STT k-ω model and applied mass flow inlet boundary conditions for the primary air inlet and fuel inlets. The outlets were treated as pressure outlets. The walls are adiabatic, meaning they do not allow heat transfer to occur between the system and its surroundings. Additionally, the no-slip condition is imposed on the walls, which means that the fluid velocity at the walls is assumed to be zero. The density of combustion air was assumed to be constant for air at 20 °C.

The specified flow rates for the inlets were provided by the cement plant and were subsequently converted to mass flow rates by the following calculations.

$$\dot{m} = \frac{\dot{Q}\rho_{t20}}{3600} \tag{34}$$

Where $\dot{m}$ is mass flow rate [kg/s], $\dot{Q}$ is flow rate [m^{3}N/h], ρ_{t20} is air density at 20 °C [kg/m^3].

The exact parameters of combustion air are given in Table 3.

Table 3 Operational Parameters

Inlet	RDF	Coal	Natural Gas	Primary Air
Flow Rate [m³N/h]	1700	2200	0	5300
Mass Flow Rate [kg/s]	0.569	0.736	0	1.773

The flow rates specified in Table 3 indicate either the flow of air itself or the flow required to convey the solid fuels to the rotary kiln. As a result, the flow rate of natural gas is 0 m^3N/h.

This simulation setup enables us to analyse the combustion air behaviour in the burner in detail and calculate the pressure drops for each combustion air branch, which is one of the intended outputs of the present work.

Simulation setup for evaluation and verification of the most eroded areas

The simulation setup utilizes the SST k-omega model combined with the DPM model. The Random Walk model is used to determine the turbulence effect of the fluid phase on the particle dispersions. The rest of the simulation settings are exactly the same as those used for evaluating combustion air (mass flow inlet, pressure outlet, adiabatic walls, no-slip conditions…).

The only distinction lies in the inclusion of an additional boundary condition known as the restitution coefficient. In a Fluent environment, this coefficient is typically defined within the wall boundary conditions. According to a study by [35], which examined the impact of pulverized coal-air mixture in the mill-duct system, the restitution coefficients associated with maximum erosion were determined to be $e_n = 0.46$ for the normal restitution coefficient and $e_t = 0.73$ for the tangential restitution coefficient. Given our objective of identifying and enhancing the areas most susceptible to erosion, these conservative values would be well-suited for our specific case.

Size of the particles

The coal particles are described using the Rosin-Rammler distribution curve (Fig. 26), which is a mathematical model used to describe particle size distribution in granular materials. Coal particles are loaded into the rotary kiln burner at a rate of *0.75 tonnes per hour* and 0.75 tonnes per hour is also fed into the secondary combustion chamber.

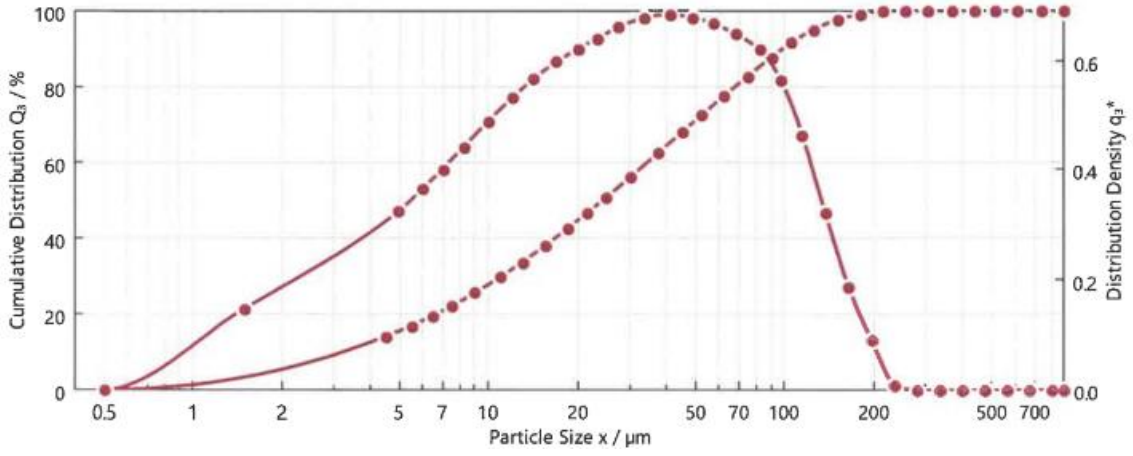

Fig. 26 Rosin-Rammler distribution curve of pulverized coal

Figure 26 provides an overview of the particle size distribution, revealing key statistics such as the average particle size of approximately 37 µm, the maximum particle size of 215 µm, and the minimum particle size of 0.5 µm. Additionally, the spread parameter is indicated to be 0.85. For a more comprehensive and precise specification, please refer to the table presented below.

Table 4 *Size distribution of pulverized coal particles*

Percentage above 1 µm = 98.23 %	Percentage above 30 µm = 43.78 %	Percentage above 63 µm = 22.00 %
Percentage above 15 µm = 62.72 %	Percentage above 32 µm = 42.03 %	Percentage above 90 µm = 12.15 %
Percentage above 16 µm = 61.09 %	Percentage above 45 µm = 31.80 %	Percentage above 120 µm = 5.74 %

6 Results and Discussion

Several simulations were performed with the aim of obtaining the desired results within this study. Let's recapitulate the objectives that were meant to be accomplished.

- Map in detail the behaviour of combustion air in the burner of the rotary kiln and just behind the burner.
- Determine the mass flow rate for the individual combustion air branches.
- Verify the erosion-stressed coal feed points and propose modifications to reduce wear.

To obtain all the mentioned outputs, it was crucial to achieve a stable solution. After undergoing numerous mesh refinements and exploring various setup options, along with approximately two months of computational time, the convergence of the solution was ultimately achieved. When encountering unstable solutions, the approach that proved effective involved reducing the time step or gradually decreasing the relaxation factors. If neither of these methods yielded success, it was necessary to redo the mesh.

Even though it may seem like an easy task, all the aforementioned processes demand a substantial amount of computational time and a certain level of experience. Even for experienced CFD engineers, achieving convergence still remains a significant challenge.

The convergence of the solution was evaluated by monitoring the essential residuals (continuity, momentum, k and ω). Additionally, the convergence of the overall pressure drop and average outlet velocity were also monitored to ensure accurate results.

6.1 Combustion air

The investigation produced the following remarkable results. As outlined in *Section 4*, the flow of primary air (combustion air) along the burner is controlled by means of butterfly valves. Initially, the simulation was performed with the intention of simulating the operation where all valves are fully opened. The accompanying image below provides a visual representation of the flow distribution within the burner under the aforementioned conditions.

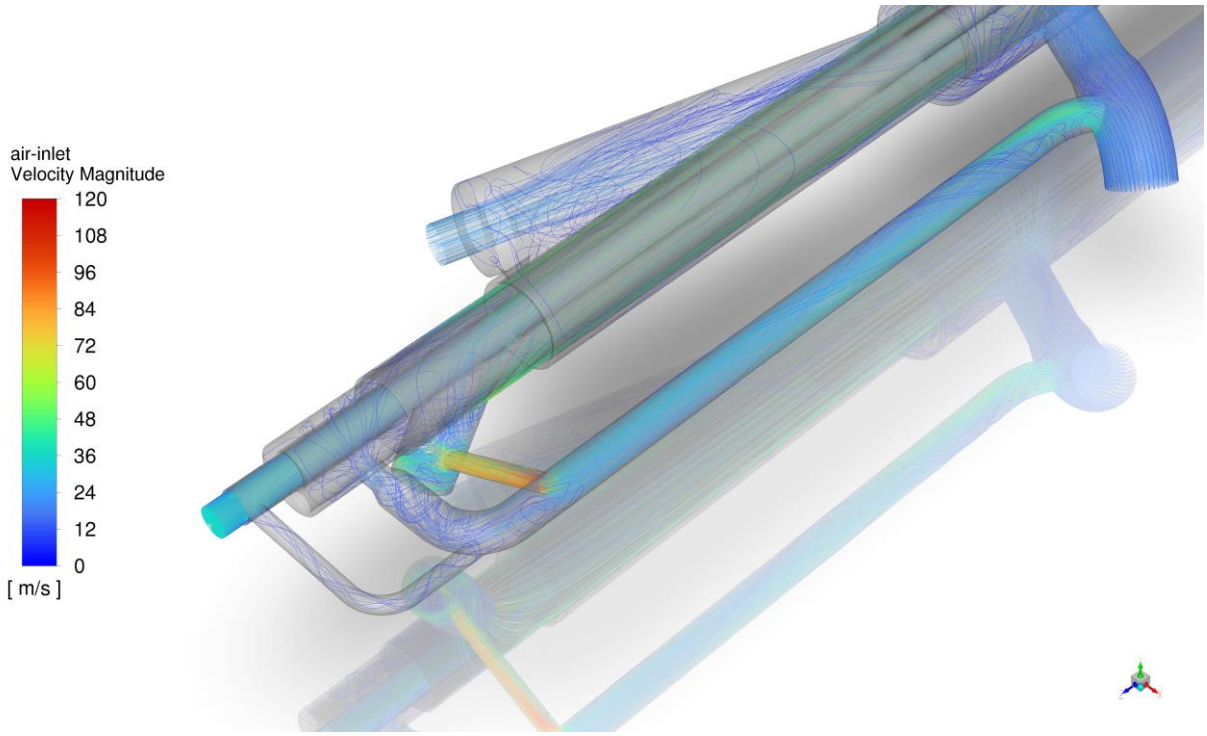

Fig. 27 *Combustion air distribution*

It is obvious that the mass flow rate throughout the natural gas cooling channel is excessive. The following table provides more detailed information about flow distribution.

Table 5 *Flow in channels with fully open valves*

	[kg/s]	[m^3N/h]	[%]
Primary air	1.152	3445	**65.01 %**
NG	0.413	1235	**23.31 %**
Central	0.178	532	**10.05 %**
Lifting RDF	0.029	87	**1.64 %**
Coal	0.736	2201	
RDF	0.57	1704	

The fluxes of combustion air within the coal and RDF channels are excluded from the rest of the group because they have their own dedicated fans which convey them through the system. The first group of flows is supplied by a primary fan which is the main source of combustion air. In the last column, the distribution of combustion air within these channels is illustrated.

Following a discussion with the cement plant, they acknowledged their awareness of the issue and confirmed that the desired flow through the pipe for effective channel cooling should be 400 m^3N/h. Subsequently, a simulation was conducted to model this desired state.

The simulation results revealed an unusually high required pressure drop across the valve in order to meet the conditions. Although it is expected that the required pressure drop should be significant, considering the presence of numerous nozzles and flow-dissipating areas in the other channels supplied by the primary air fan (as illustrated in the accompanying picture), the

observed pressure drop remains notably elevated. The more in detail explanation is provided below.

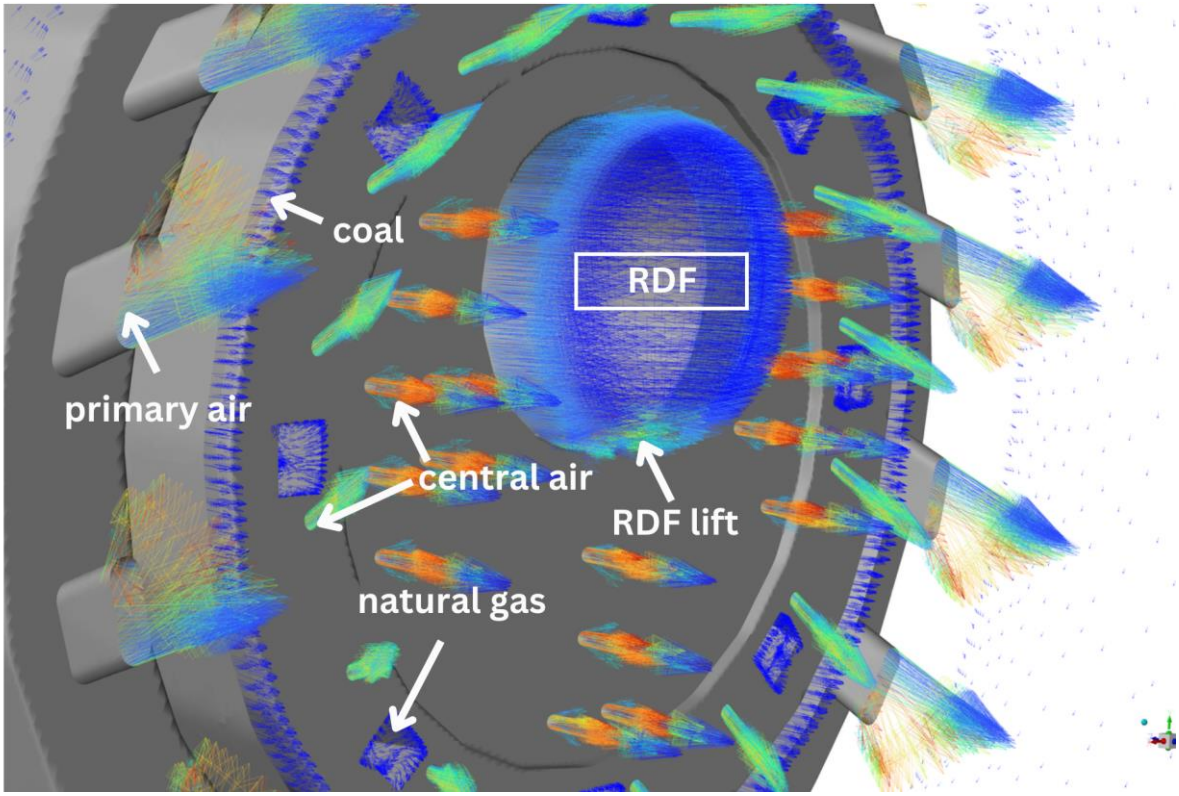

Fig. 28 *Kinetic energy of turbulence at the outlets*

Fig. 28 is a vector representation of turbulence kinetic energy at the outlets. A high turbulence kinetic energy (TKE) value indicates that a significant amount of energy is associated with turbulent fluctuations in that particular area or region of the flow. Therefore, a high TKE value typically indicates a higher level of turbulence and greater energy expenditure in that specific area of the flow field.

In our case, we already know that the primary air fan supplies several channels, including the primary air channel, RDF lifting channel, central air channel, and the natural gas channel. The remaining fuel channels have their own dedicated fans for conveying fuel or particles within the system.

From *Figure 28* it is evident that the TKE values are significantly higher in the RDF lifting channel, primary air channel, and central air channel compared to the natural gas channel. This discrepancy suggests that the pressure drop in these channels is greater than that of the natural gas channel. Consequently, the flow tends to favour the path of least resistance, leading to a preference for the natural gas channel.

This serves as evidence that in order to decrease the flow within the natural gas cooling channel, it is necessary to employ a regulating valve that would generate a substantial pressure resistance across it. The intention is to create a pressure resistance significant enough that the flow would choose to pass through the other channels (at least partially), which already possess considerable pressure resistance. However, it is worth noting that despite taking this into

account, the resulting pressure resistance required to attain the desired flow through the natural gas channel remains exceptionally high.

Significant time and effort were dedicated to identifying the underlying problem. However, it must be acknowledged that the time allocated for this complex CFD simulation is insufficient, given the circumstances. To start this investigation, it was necessary to wait until the burner was dismantled to obtain the necessary measurements. Also, the final model itself comprises 25 million elements, which has already undergone substantial reduction. These factors contribute to the substantial computational time required, which exceeds the scope of a thesis. Consequently, in light of these considerations, further investigation into the cause of the excessively high required pressure resistance across the valve as a potential future research subject is recommended.

The main objective of this study was to comprehensively map the combustion airflow behaviour within the burner. The obtained results will be utilized to effectively illustrate the internal processes taking place within the burner. Despite the higher required pressure resistance across the valve needed to regulate the natural gas cooling channel, the obtained results still provide a comprehensive description of the processes occurring within the burner. The detailed mapping of the flow behaviour allows for a thorough understanding of the burner's operation and provides valuable insights into its performance.

The following section will outline the approach to optimizing the valve opening angle in order to achieve the desired pressure resistance across the valve.

At first, it is necessary to establish the relationship between the pressure resistance and the angle of the open valve. However, this practice is not widely adopted in the industry. Usually, the valves are described by a value of "Cv", which indicates the liquid flow rate required to generate a pressure drop of 1 bar.

We have obtained this specific characteristic of the valve (used in the natural gas (NG) cooling channel) from the valve supplier (tab. 6). Additionally, from the onsite measurement, we knew that the diameter of the NG channel is 80 mm.

Tab. 6 *"Cv" values for different butterfly valve sizes*

Cv values m³/h

	opening angle of the valve							
Sizes	20°	30°	40°	50°	60°	70°	80°	90°
32		1,5	5	10	15	26	34	40
40		2,7	8,5	16	25	37	46	50
50	2	7	15	28	45	68	88	100
65	3	11	24	48	85	138	180	210
80	8	22	50	83	134	230	312	360
100	15	35	70	130	225	410	585	650
125	28	70	135	230	360	600	920	1050
150	33	95	205	320	580	980	1410	1620
200	60	175	355	580	910	1600	2450	2800
250	132	340	590	940	1480	2550	3950	4480

Fig. 29 *Butterfly valves used in the burner channels*

Since the information provided by the supplier was limited by Table 6, additional calculations had to be performed to obtain the required dependence.

The calculation method employed involved combining the flow rate, Cv value, and the desired outcome of achieving a specific pressure drop. The modified form of the equation has the following format [34].

$$\Delta p = \frac{\left(\frac{\dot{V}}{Cv}\right)^2}{\rho} \tag{35}$$

Where $\dot{V}$ is flowrate in [m^3/h] (required flowrate for efficient cooling of NG channel is 400 m^3/h), Cv is the flow of liquid that will create a pressure drop of 1 bar and ρ is the density of the fluid in [kg/m^3].

From here, it became possible to establish the subsequent dependency. It is important to note that the provided graph is only applicable to a mass flow rate of 400 m^3N/h. For any other flow rate, the dependency would vary.

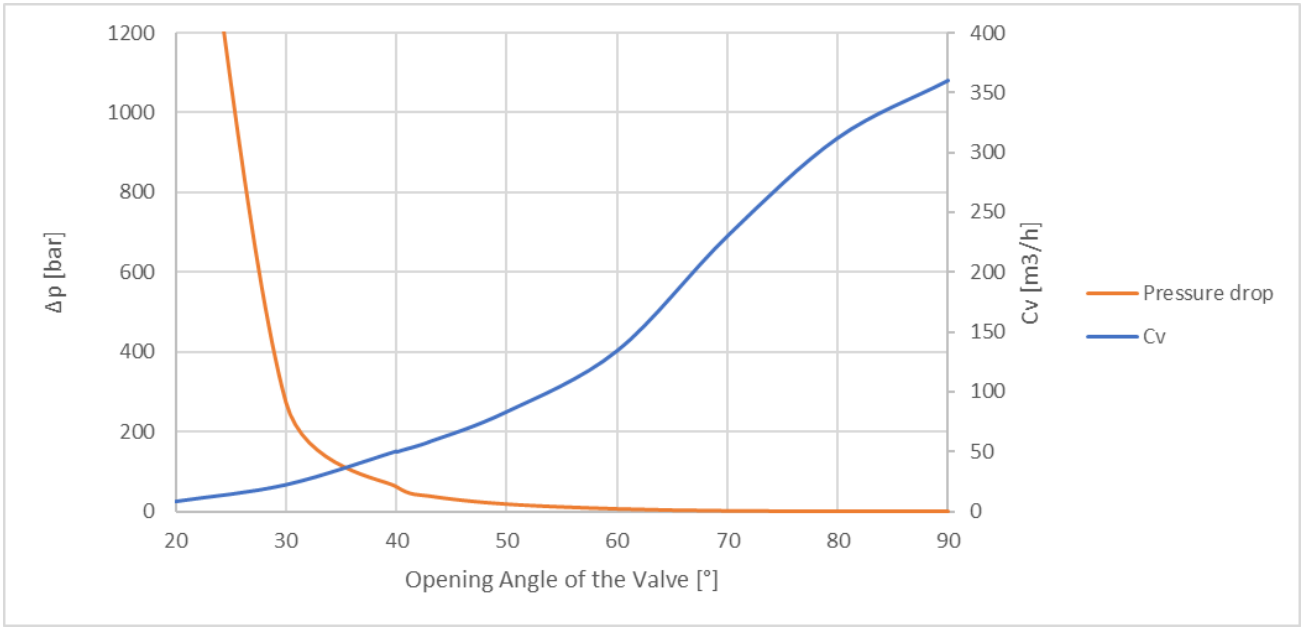

Fig. 30 *Valve opening angle dependency*

For a clearer visualization, a scoped graph is provided below.

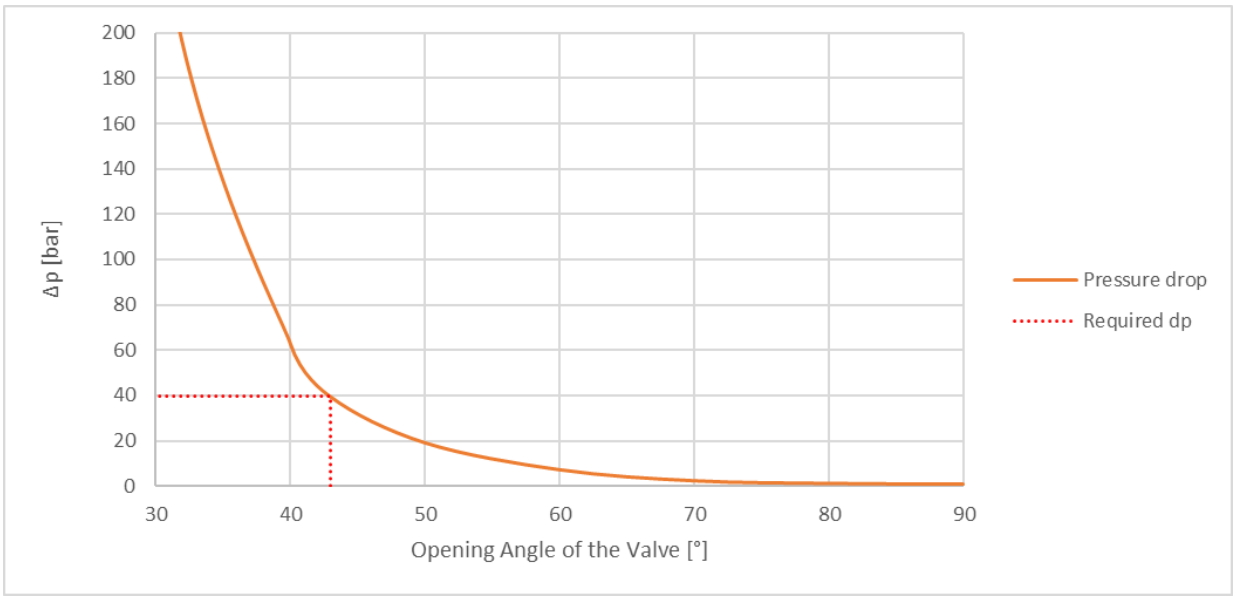

Fig. 31 *Required valve opening angle*

From Figure 31, it can be determined that in order to achieve the desired operational conditions, the valve should be opened to an angle of 43°.

With an optimized system like this, the burner, and specifically the combustion air, possess the following parameters.

Table 7 *Flow distribution in channels with the required mass flow rate*

	[kg/s]	[m^3N/h]	[%]
Primary air	1.386	4144	**78.17 %**
NG	0.134	401	**7.56 %**
Central	0.216	646	**12.18 %**
Lifting RDF	0.037	111	**2.09 %**
Coal	0.736	2201	
RDF	0.606	1812	

The same as before applies, the last column in the Tab. 7 represents the distribution of the combustion air supplied by the primary fan.

A representation of the flows throughout the burner can be seen in the following figures. It is clear that the flow inside the natural gas cooling channel has been properly optimized.

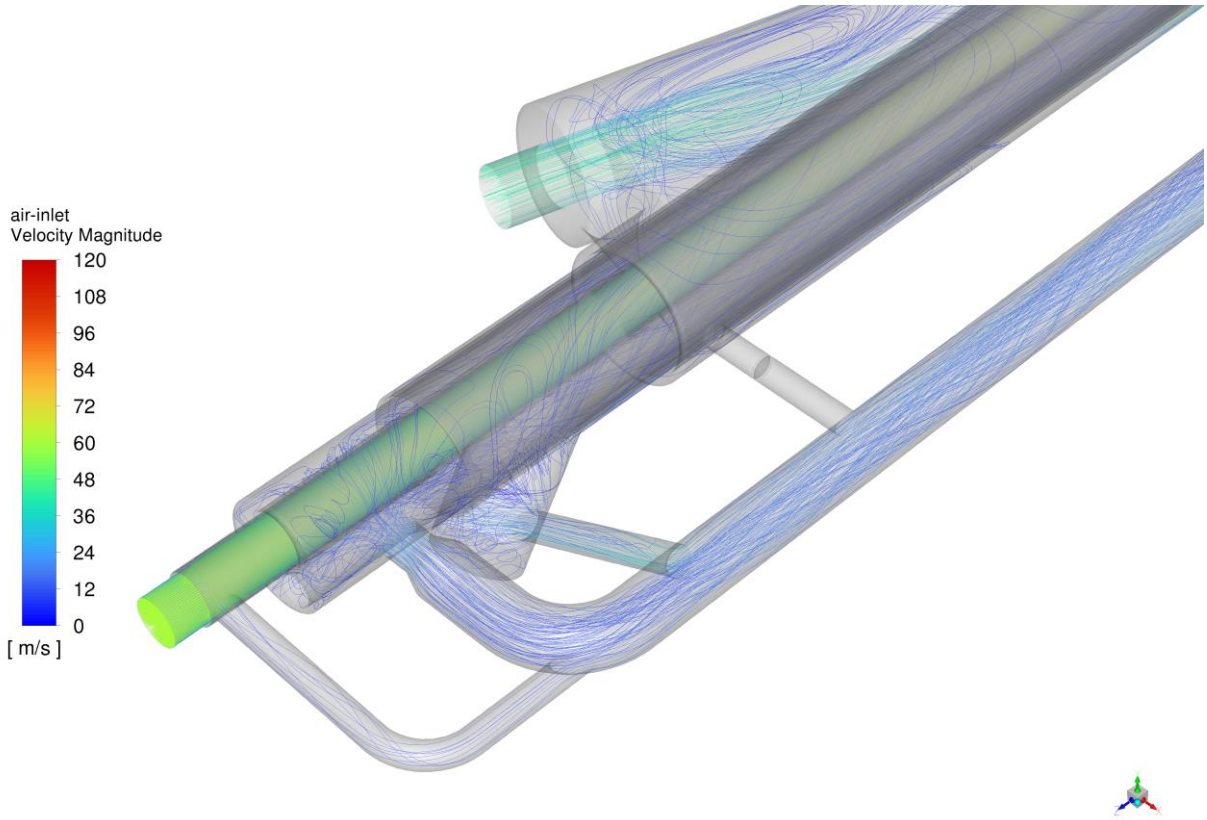

Fig. 32 *Combustion air distribution - regulated*

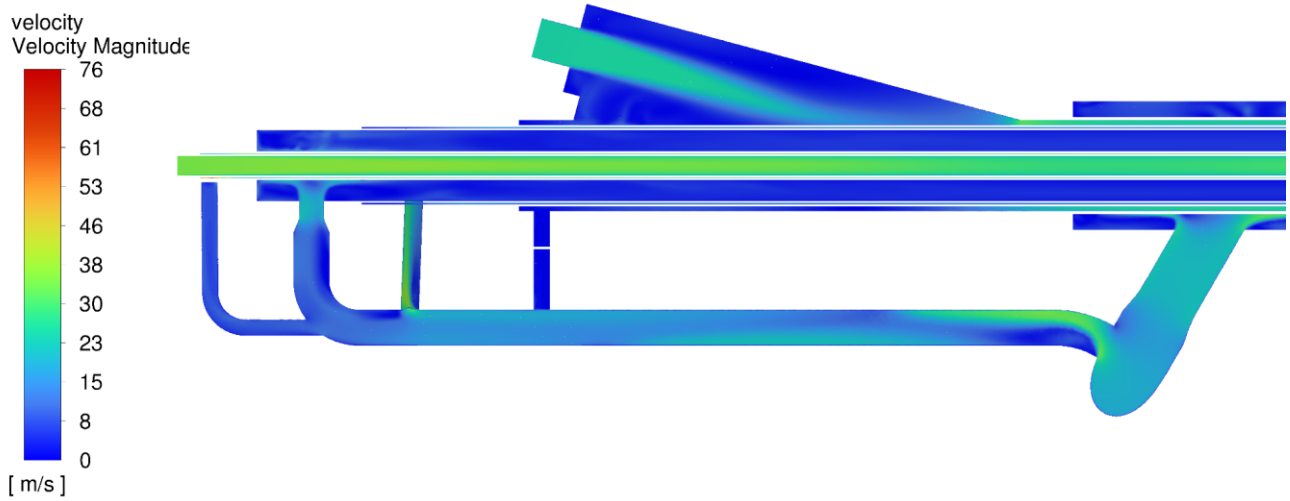

Fig. 33 *Velocity contour of the back of the burner*

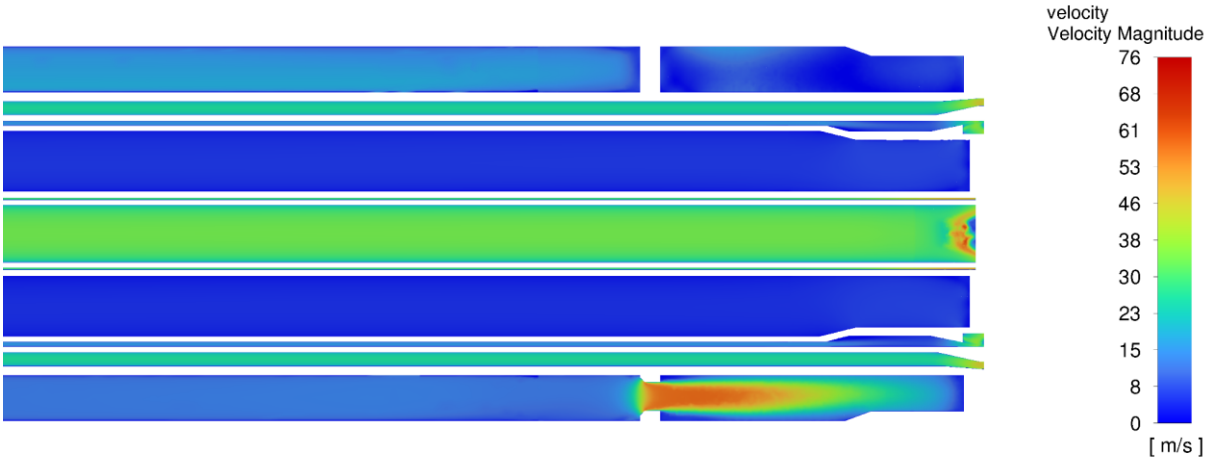

Fig. 34 *Velocity contour of the front of the burner*

In Figure 34, the attached scale map is not properly adjusted, as the intention was to emphasize the specific area where the change is occurring while maintaining uniform contours for effective comparison. The proper figures are provided in the following section (*"Combustion air behind the burner"*), where a more comprehensive depiction of the flow at the outlets and immediately behind the burner can be illustrated.

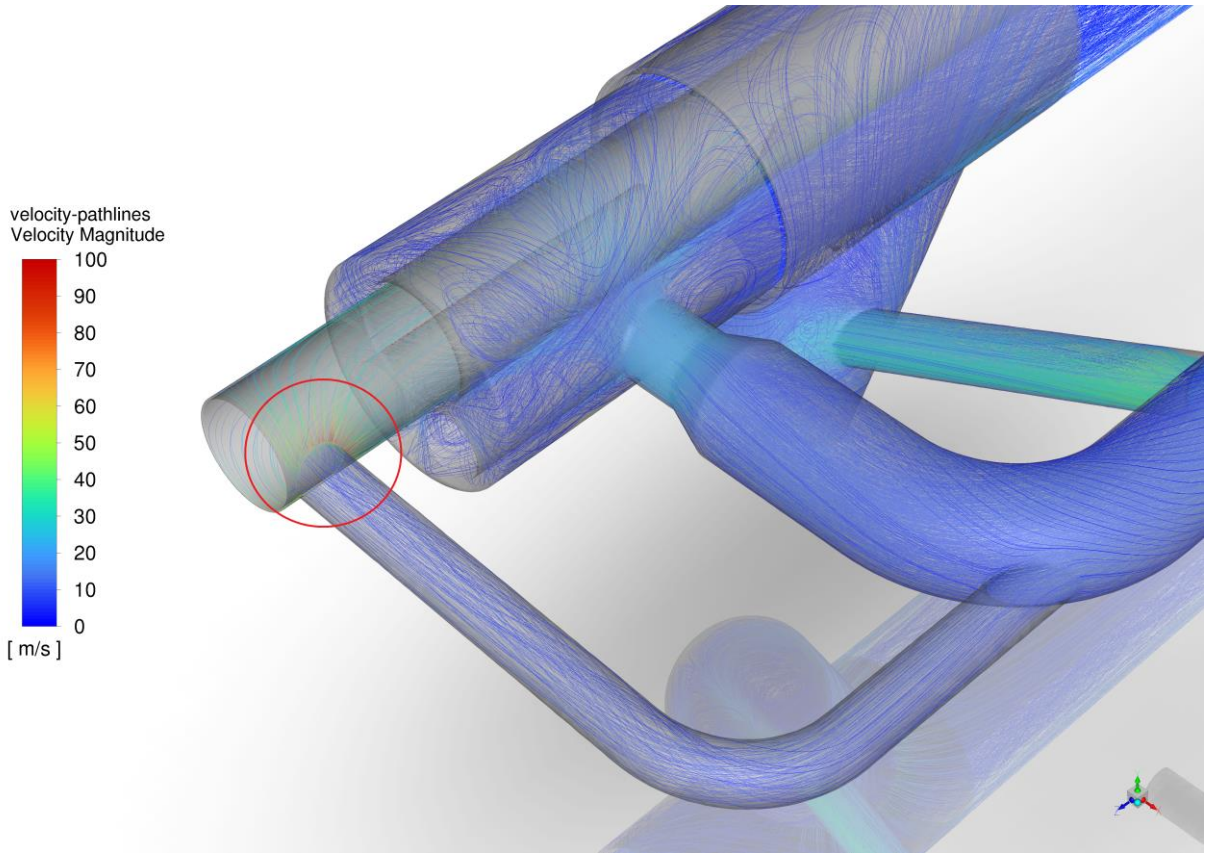

Fig. 35 *Cooling channel of RFD lifting pipe*

Another finding from the simulation is the high velocity observed in the RDF lifting channel (Fig. 35). This is attributed to the sudden change in space (Bernoulli's principle). The speed can be reduced using the same approach applied to the natural gas cooling channel, by appropriately optimizing the valve opening. However, it should be noted that in the simulation, there is currently no valve present. Since the mass flow in this channel accounts for only 2 % of the total combustion air supply, the resulting change would not be considerably significant. Therefore, conducting another simulation is unnecessary as it is time-consuming. The recreation of the real flow of combustion air can be considered accurate and valid.

Another area of interest is the region surrounding the plate depicted in the Figure 37. The plate serves the purpose of accelerating the flow before it passes through the subsequent nozzles. The situation is further illustrated in the accompanying images below.

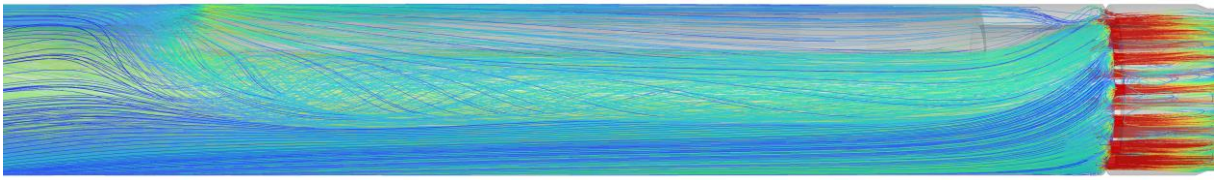

Fig. 36 *Primary airflow around the plate – side view*

Fig. 37 *The plate in the real kiln burner*

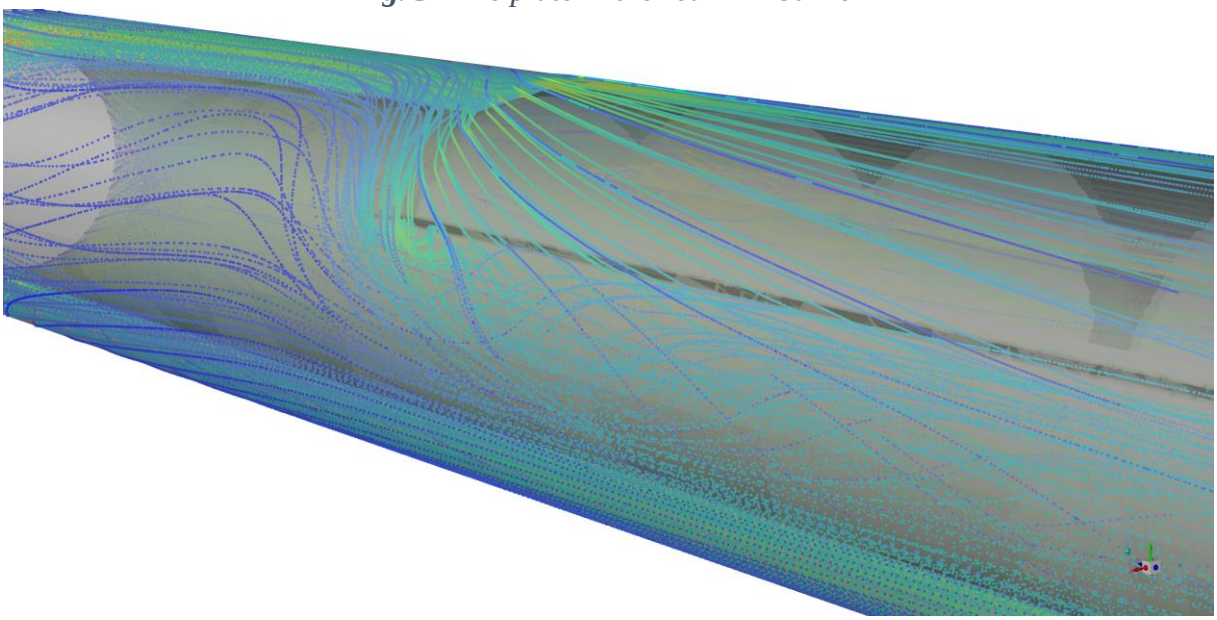

Fig. 38 *Detailed look at the airflow around the plate*

The aforementioned pictures clearly demonstrate that the plate fulfills its intended function effectively.

Another aspect worth mentioning is the decrease in efficiency observed at each inlet to the respective channel. As illustrated in the figure below, the formation of eddies in the rear section of the primary air channel contributes to reduced efficiency. While the elongated design of the rear section serves a purpose from a design standpoint, incorporating flow directors would likely enhance the overall efficiency.

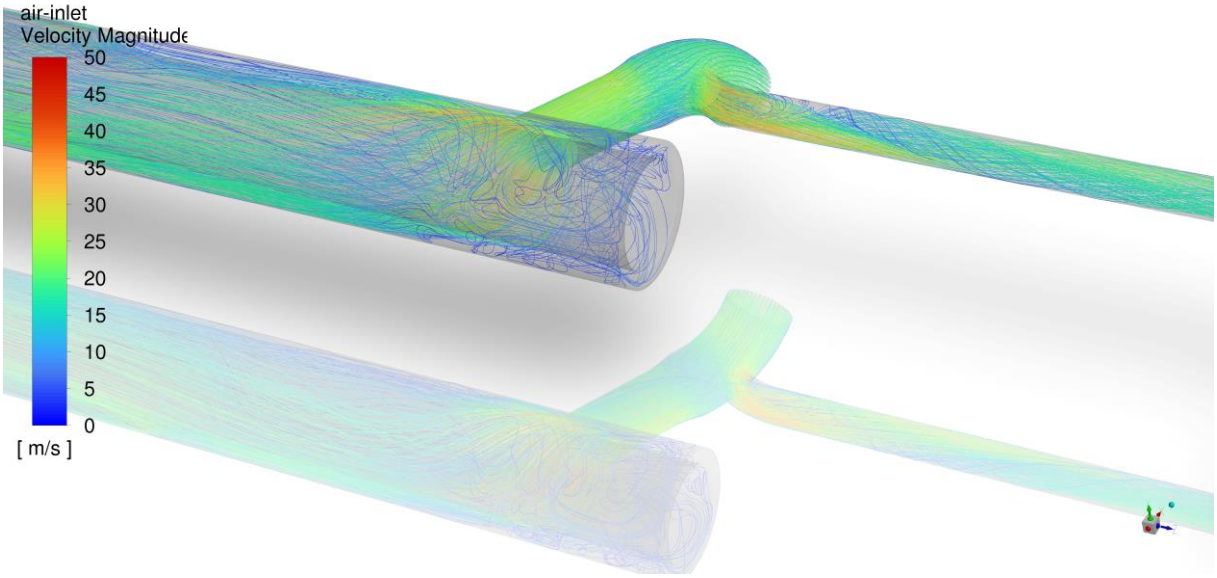

Fig. 39 *Formation of eddies at the inlet to the primary air channel*

Combustion air behind the burner

Figure 40 illustrates that the maximum velocity at the outlet nozzles reaches approximately 250 m/s. The figure also demonstrates the mixing of combustion air behind the outlet. To visualize this, pathlines of velocity were generated. In addition to the swirling flow of combustion air, secondary air entering this region will contribute to further mixing.

For a comprehensive understanding of the exit velocities from the nozzles, please refer to Figures 40, 41, 42 and 43. This visual representation allows us to observe the directions and velocities of combustion air leaving each nozzle, providing insight into what nozzles contribute to the swirling flow (adjustable primary air nozzles as well as the outer part of the central air outlet nozzles).

The two vacant areas below the RDF outlet remain unused as they were intended for oil fuels. However, the current operation of the cement plant does not employ this approach.

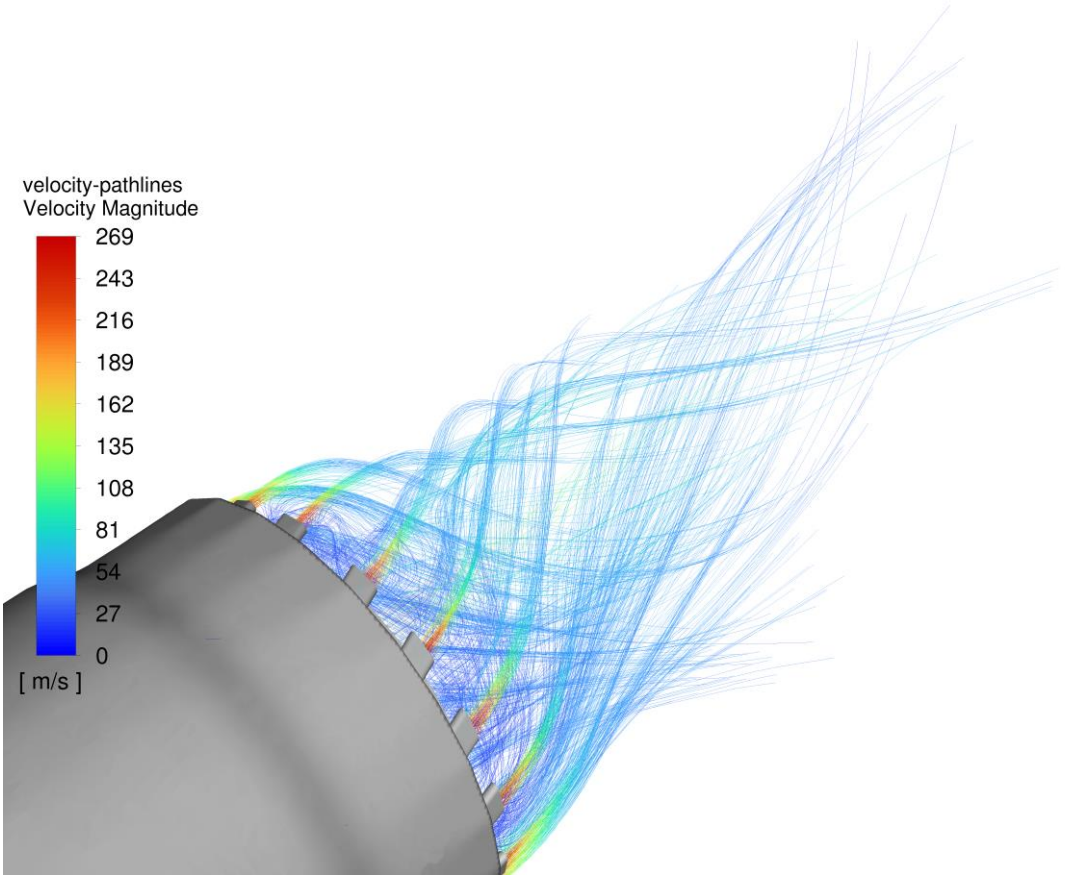

Fig. 40 *Swirling flow behind the burner*

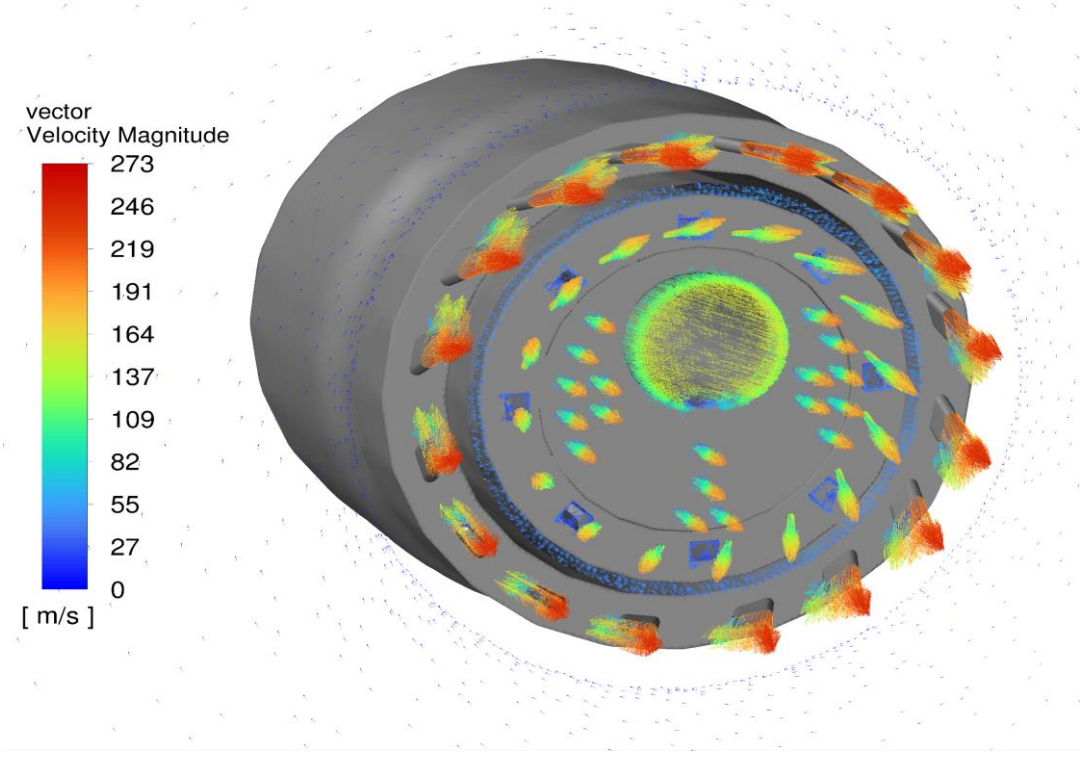

Fig. 41 *Vector representation of outlet velocities*

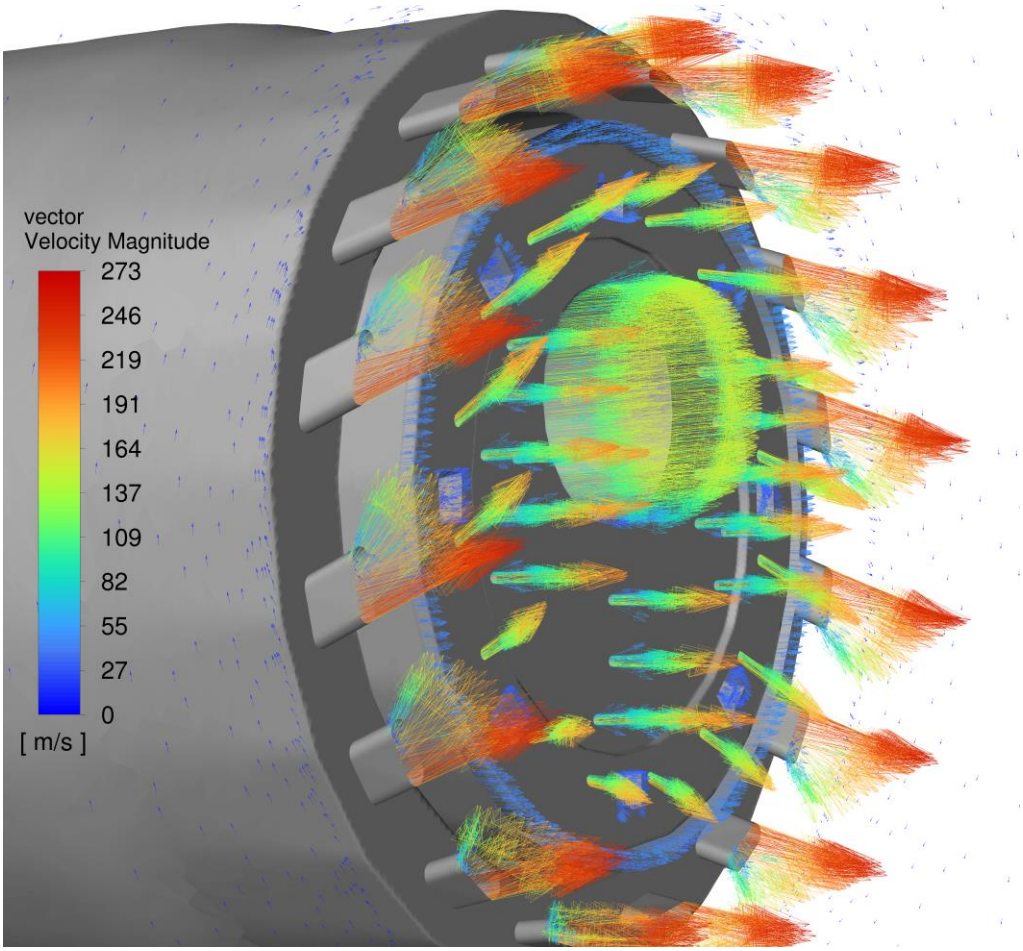

Fig. 42 *Side view of output velocity vectors*

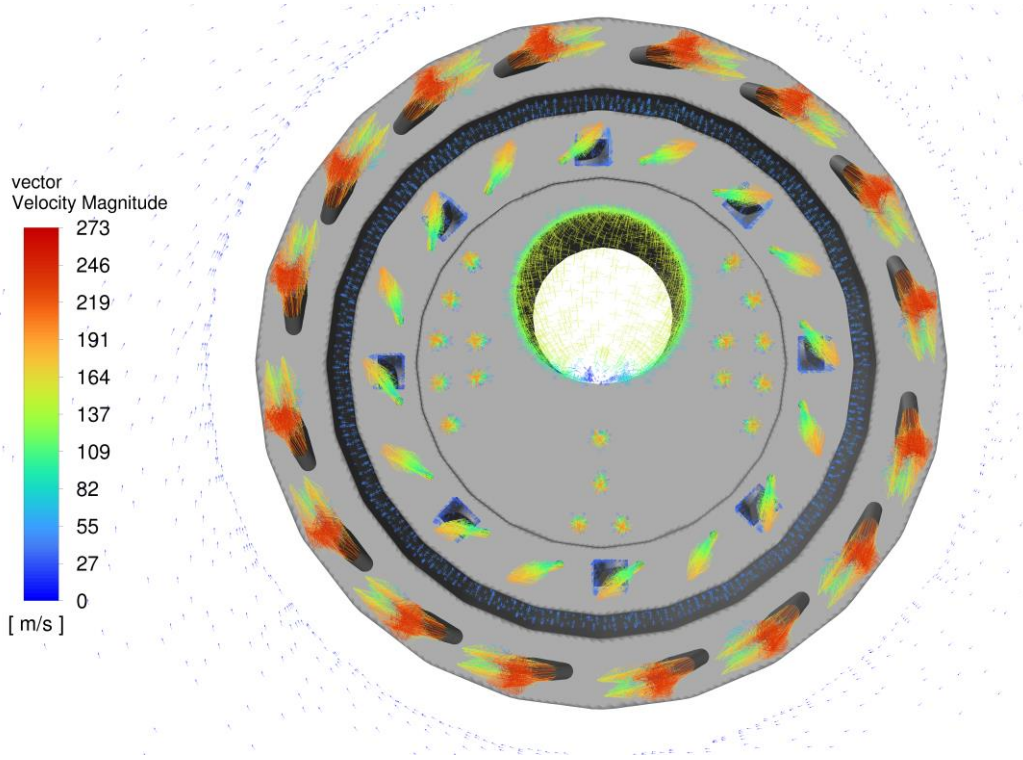

Fig. 43 *Front view of output velocity vectors*

Another noteworthy aspect worth mentioning is the presence of a specific holes, discussed in *Section 4.1* regarding *Model Creation*, designed to enhance the upward lift of RDF fuel inside the kiln. A more comprehensive understanding of this situation is provided through the inclusion of figures showcasing the findings from the CFD analysis. These visual representations offer valuable insights into the effects and behaviour of the RDF fuel within the kiln.

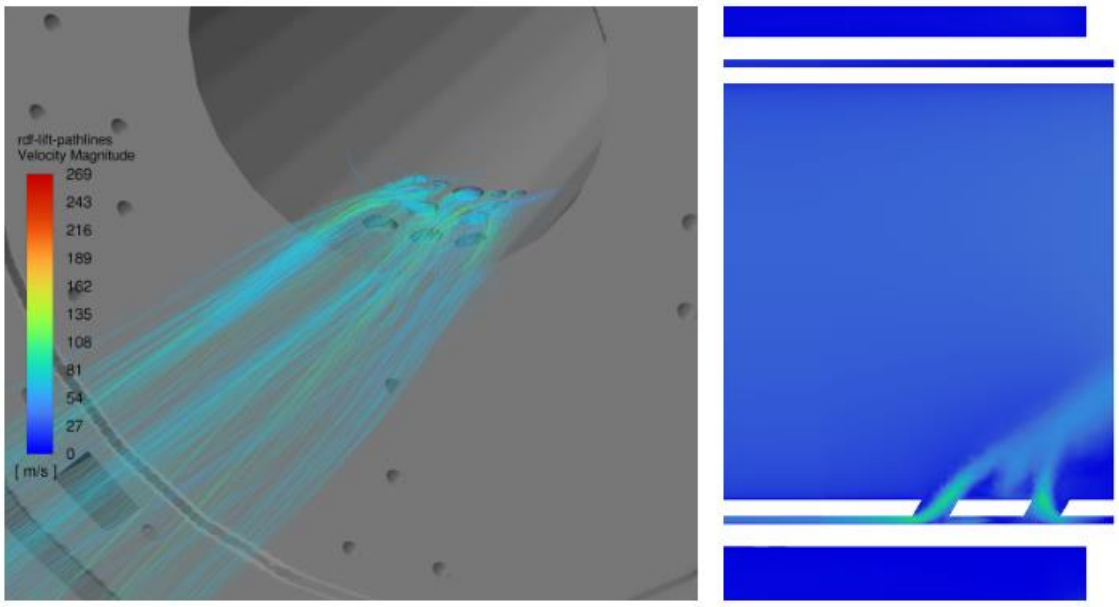

Fig. 44 *RDF lifting holes from both a 3D perspective and a cross-sectional view*

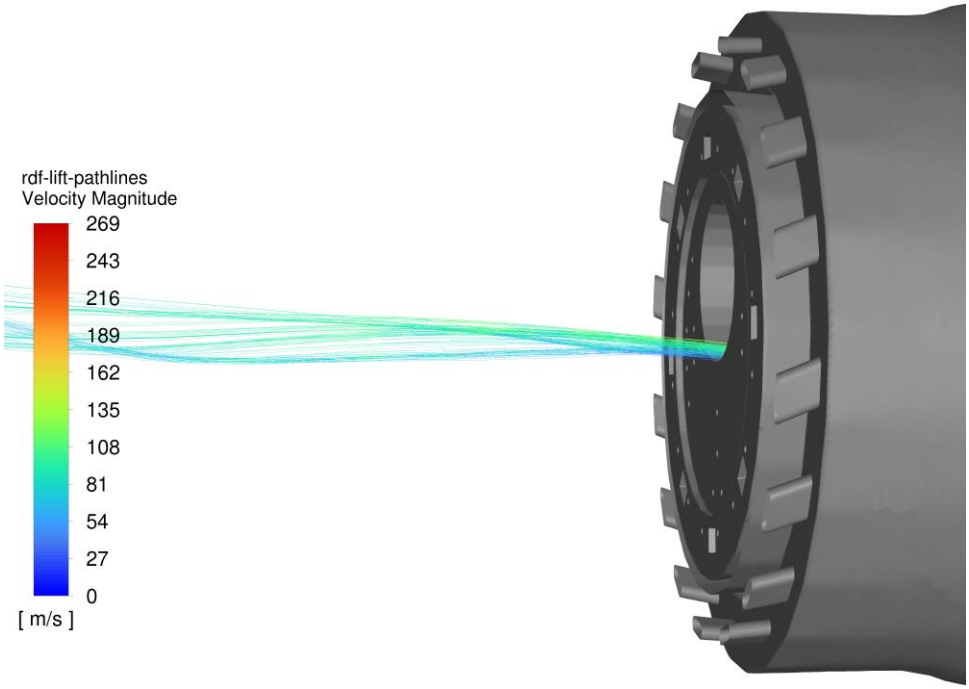

Fig. 45 *RDF lifting channel pathlines after the outlet*

While the impact of the lifting holes may appear negligible, it is important to note that their effectiveness is compromised by simulating only the combustion air flow. In actual operating conditions, the RDF channel would be filled with RDF fuel, creating resistance for the fluid to leave the RDF lifting channel. This resistance would lead to an increase in pressure, which would later become an essential force for lifting the RDF particles further into the kiln.

Swirl Number

The most crucial parameter obtained from this simulation in this particular section is the swirl number. To summarize, the swirl number in burners is a parameter that quantifies the degree of swirling motion in the flow. It is a dimensionless quantity calculated by dividing the tangential velocity component by the axial velocity component. The swirl number provides valuable information about the rotational flow characteristics within the burner and is often used to assess and optimize combustion performance. A more detailed description is provided in section *2.4 Swirling flows*.

It is important to note that the radius used in calculating the swirl number is only 0.8 m, whereas the radius of the actual kiln is larger. As a result, the swirl number would differ. Another point to consider is that in the actual operation, the role of secondary air in the mixing of combustion air is crucial. However, it was not considered in this study, which means that the resulting swirl number would be significantly different in real-world conditions.

The intention was to illustrate the potential relationship between the swirl number and the distance from the outlet. The following figure combines the velocity contour behind the burner with the dependence of the swirl number on the distance from the burner.

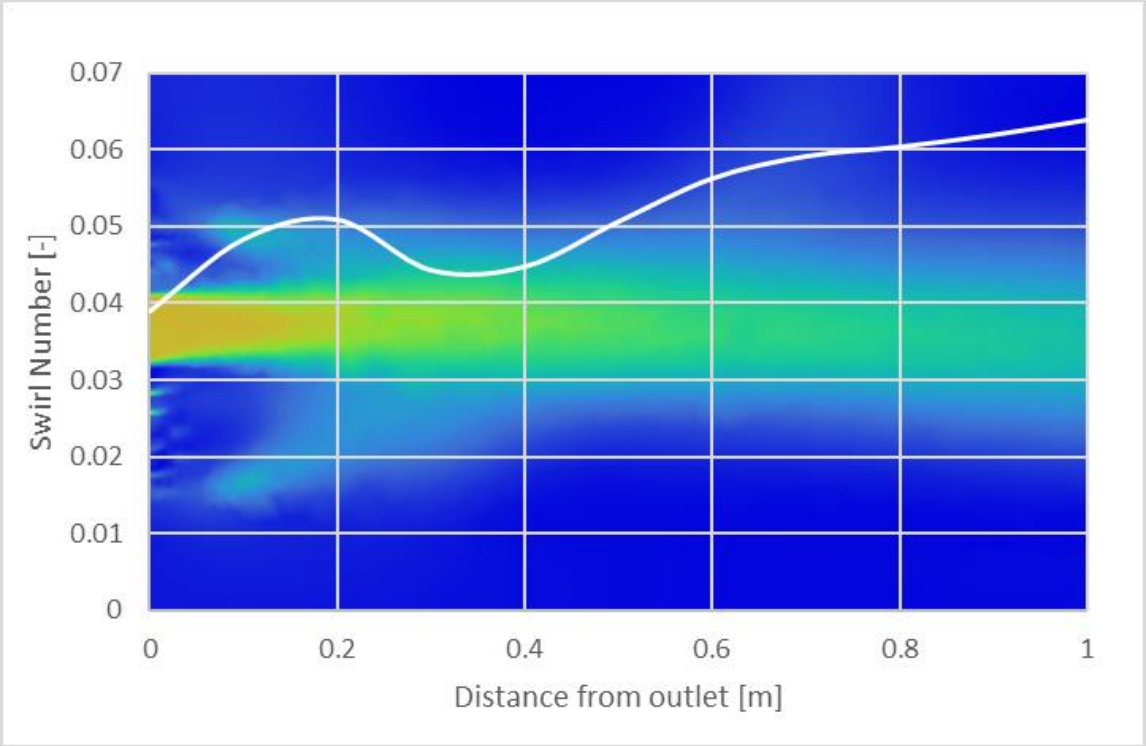

Fig. 46 *Dependence of the swirl number on the distance from the outlet*

6.2 Erosion by coal particles

The last objective of this work is to investigate and verify the erosion stresses on the coal feed points, which is crucial in the efficient operation of rotary kiln burners. The outcomes are expected to contribute to the understanding of the erosion phenomena and help improve overall operational efficiencies. In addition, ways to mitigate the impact of pulverized coal particles and minimise erosion damage within the rotary kiln burner are also proposed.

Fig. 47 *Damaged pulverised coal channel - Eroded area*

Based on Figure 47, it is evident that this issue demands significant attention. The image showcases a disassembled burner from the cement plant. By conducting the simulation, we can gain a comprehensive understanding of the erosive effects that occur during operation. Consequently, we can propose an efficient particle guidance system to provide adequate protection against erosion. While the damage caused may not be critical, implementing an appropriate system setup would be beneficial in reducing maintenance costs.

To be aware of the precise location of the eroded area (the area behind the pulverized coal feed point), the figure below is provided. This schematic drawing represents the configuration of the actual burner.

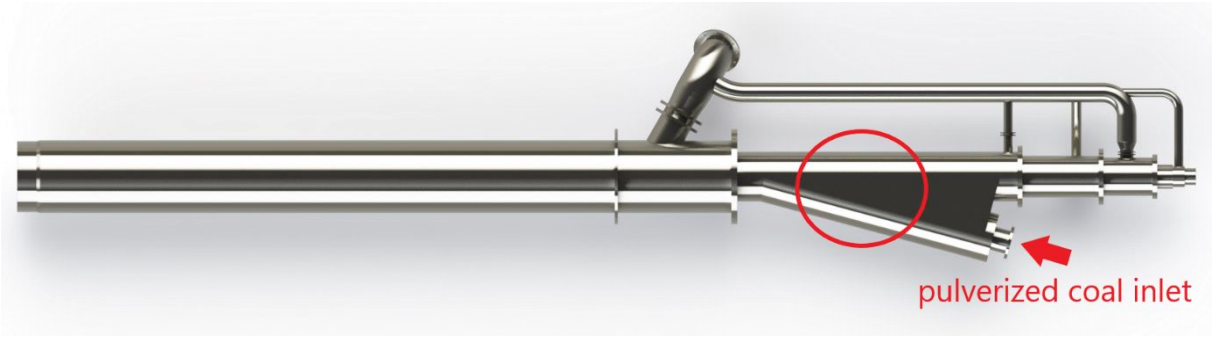

Fig. 48 *Schematic representation of the most eroded area (top view)*

After the simulation was prepared once again, but this time considering the particles of pulverized coal, a better understanding of the flow of the air-coal mixture was obtained. Once the solution converged, the steady-state system and erosional action on the burner could be illustrated through the following figures.

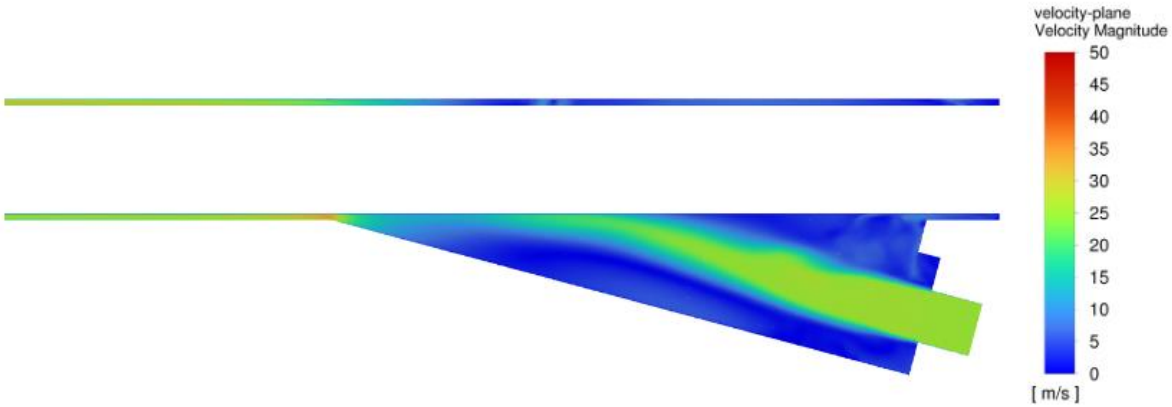

Fig. 49 *Velocity contour of the rear part of pulverised coal channel (cross-section view)*

Figures 48 and 49 can now be compared to gain a better understanding of the internal dynamics within the coal channel. Figure 49 illustrates the flow of the combustion air and pulverized coal mixture, the area where particles impact the pipe, and provides a visual representation of the flow velocity.

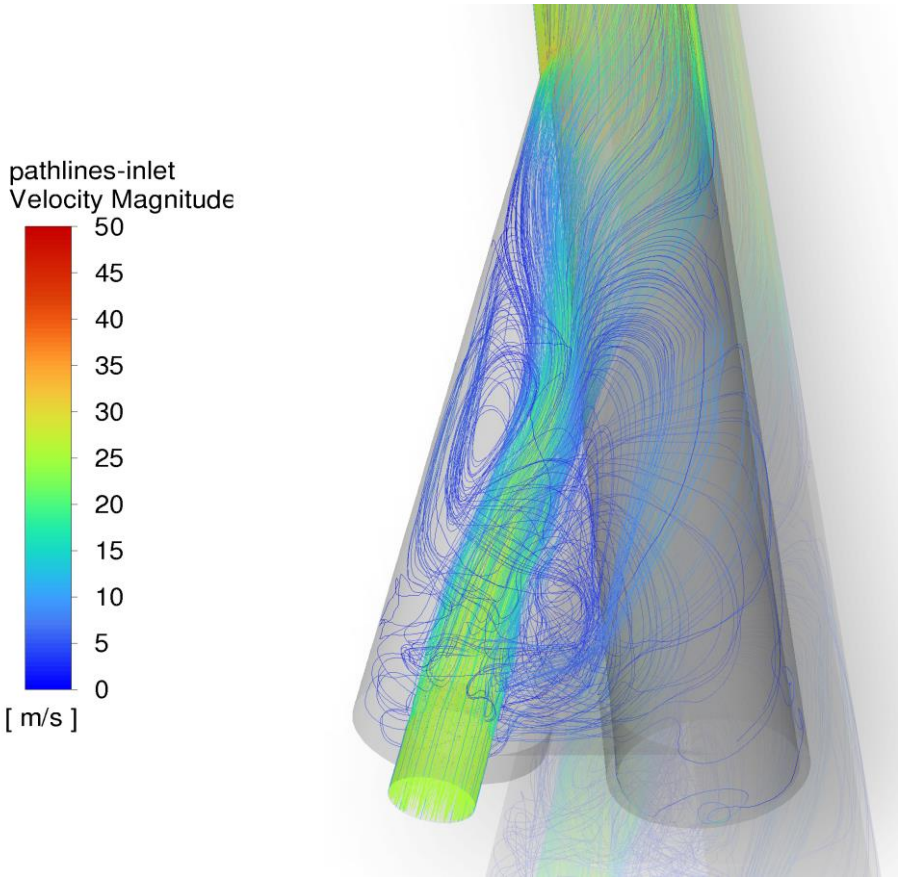

Fig. 50 *Visualization of coal-air mixture pathlines*

Figure 50 presents an alternative schematic representation from a different angle. It provides an additional perspective, allowing us to observe areas where small turbulent eddies could potentially form, leading to an increased risk of erosive wear in those regions.

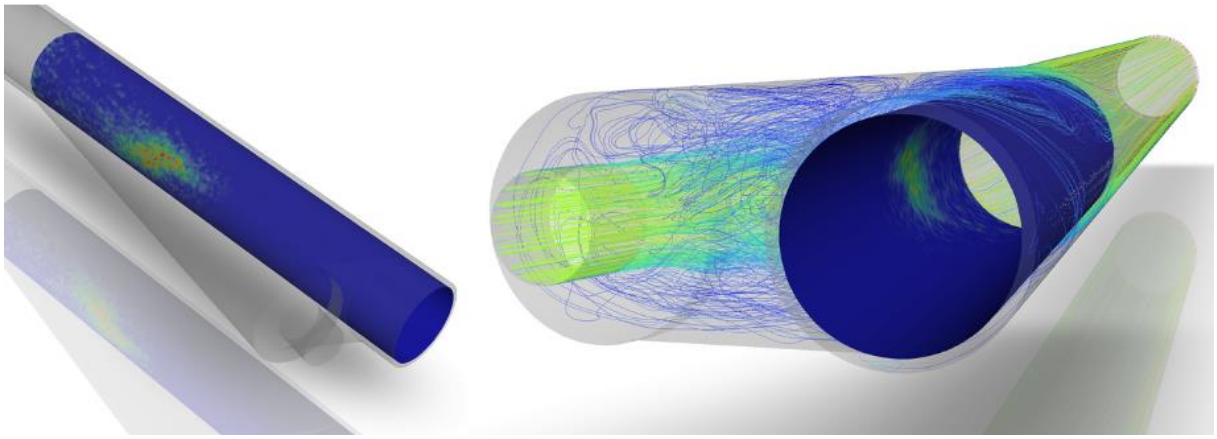

Fig. 51 *Erosion-stressed area*

The evaluation of erosional action is carried out by using *The Finnie Model*, as described in *Section 3.2.3 - Erosive Action*. The precise value of erosion is not of particular interest to us, as we are not considering specific materials, meaning the associated scale map is not required. What holds significance for us is identifying the areas where particles tend to accumulate most frequently.

From the pictures above combined with analysing the completed simulation, it has become evident which specific areas have sustained the most significant damage. These areas represent the points where the particles from the pneumatic conveying system come into contact with the pipe. They should now receive primary focus and attention. Before presenting an erosion protection system, it is important to consider some key factors. As highlighted in [37], the maximum erosion for steel is assumed to occur at an angle of particle impact of 45°. Keeping this in mind is crucial when suggesting any adjustments for erosion protection.

Furthermore, an additional simulation was performed with new particles that make up 1 % of all particles, with a size of 500 µm, which is 2.5 times larger than the maximum particle size in the last simulation. The idea behind the simulation was to verify if the erosion-stressed area would shift to a potential region (Fig. 52) where larger particles entering a narrowed channel could lead to excessive erosion. This scenario of larger particles in the system could occur if there were any errors during the grinding process, causing the particles to not reach the required fineness.

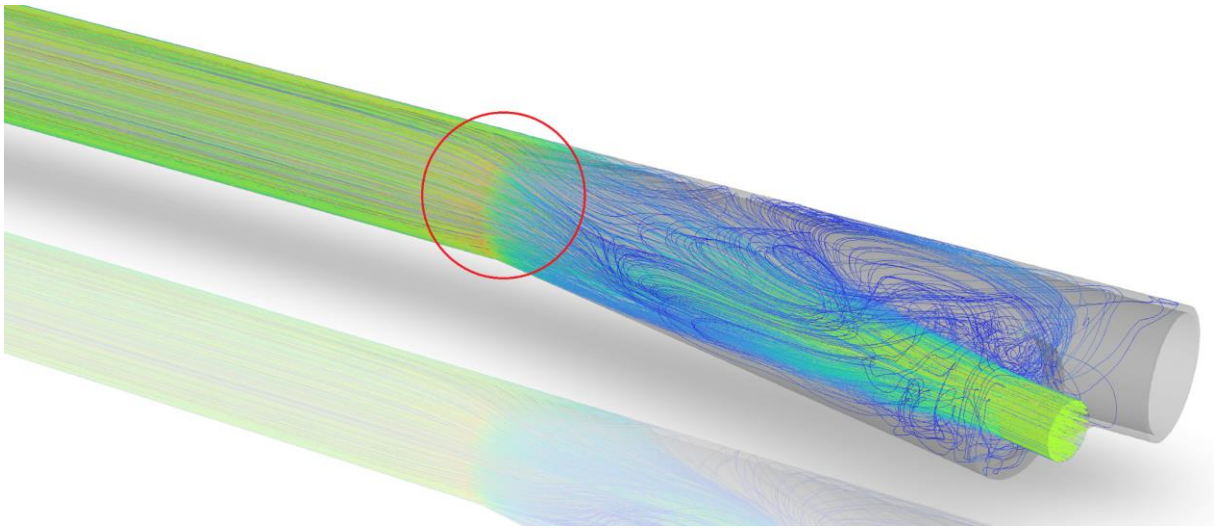

Fig. 52 *Potential region with excessive erosion*

Figure 53 below represents the results. It clearly indicates that the area experiencing erosive stress corresponds to the region of particle impact. Furthermore, the analysis reveals that the presence of slightly larger particles, accounting for less than 1 % of the total particles, does not have a significant impact on erosion. With these findings in mind, we can now move forward and propose an effective erosion protection system.

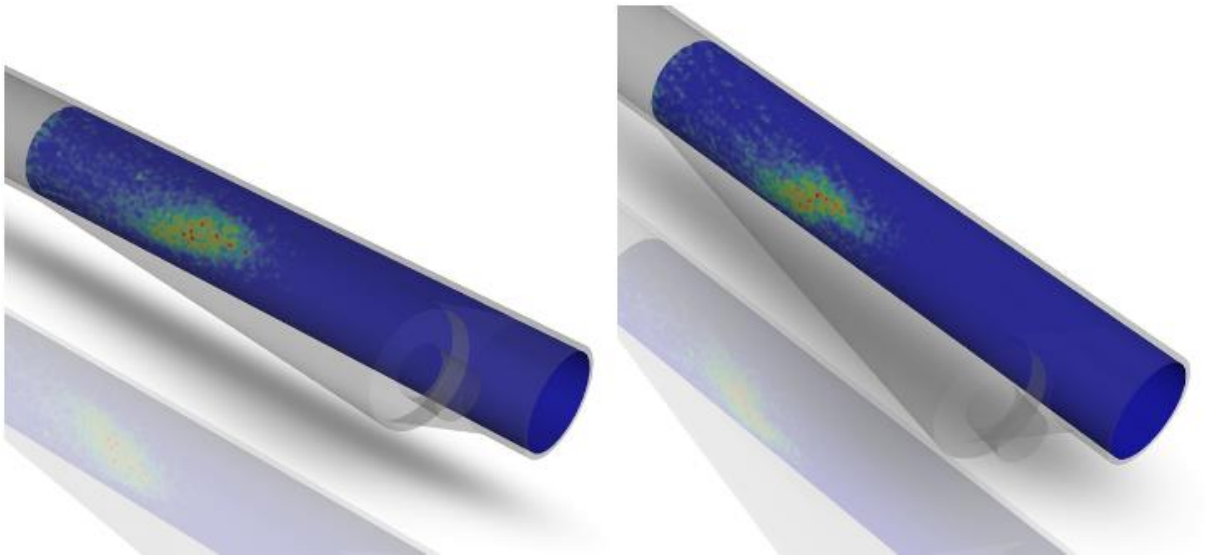

Fig. 53 *Comparison of the erosive effects (left - larger particles, right -normal particles)*

Erosion protection system

Erosion protection systems encompass a range of applications and techniques that can be utilized to safeguard pipes from erosion. The selection of a suitable system depends on various factors such as financial resources, the specific application, and the type of particles flowing inside the pipe. Commonly employed erosion protection methods in industrial settings include coatings, linings, velocity control devices, streamlined designs, and more. Each of these approaches offers unique benefits and considerations, allowing for tailored solutions to mitigate erosion effectively.

In our specific case, it is desirable to introduce and utilize an approach that does not interfere with the design of the burner itself but focuses on adjusting the pipe system prior to the burner inlet. This approach is preferred due to its ease of implementation. One viable solution that aligns with these requirements is the implementation of a particle routing system. By employing a particle routing system, we can address the previously mentioned particle impact concerns, specifically the need to avoid angles around the critical 45° angle.

The concept of a particle routing system entails the integration of key components within a pipe to effectively guide and control the movement of particles. These components can include deflectors, baffles, flow straighteners, vortex breakers, and internal coatings. Deflectors are strategically placed to redirect the particle trajectory away from critical areas, while baffles disrupt the particle flow to dissipate energy and reduce impact. Additionally, internal coatings can be applied to enhance the pipe's resistance to abrasion and erosion. By incorporating these components into the particle routing system, we can create a comprehensive and efficient solution to protect against erosion and prolong the lifespan of the system.

7 Conclusion

This thesis was conducted in cooperation with a cement plant Českomoravský cement, a.s., Mokrá facility. As part of the research process, a visit to the plant was arranged. During this visit, open discussions were held with an experienced cement plant engineer to gain valuable insights into the detailed processes involved in cement production, particularly focusing on combustion air within the burner. These were the essentials before proceeding further.

Following the discussions, multiple measurements were carried out on two different burners. These measurements served as essential data for constructing a real-life model of a cement rotary kiln burner. The model then underwent validation and approval by the cement plant.

Subsequently, extensive preparations were conducted for the forthcoming simulations. This involved removing unnecessary design elements, and simplifying and optimizing the model to achieve optimal results while minimizing computational time. Additionally, a hybrid mesh was created for the simulations, as attempts to generate a single uniform mesh of desired quality were unsuccessful.

Simulations were conducted with the aim of drawing various conclusions. The first simulation focused on mapping the detailed behaviour of combustion air inside the burner. This analysis revealed areas where the combustion air was reaching excessive velocities and identified specific regions that needed regulation in order to achieve the desired outcome parameters. Further investigation was conducted to optimize the combustion air flow of the burner, addressing the identified errors.

During the annual maintenance checks and repairs of the burner at the cement plant, it was observed that a specific area was prone to excessive wear. Therefore, another analysis was conducted to specifically investigate the erosive wear effects occurring behind the pulverized coal inlet. Through the simulation and the subsequent analysis of the results, various strategies to reduce wear in erosion-prone areas were suggested. The proposed approaches are expected to provide an effective solution for reducing erosion.

In conclusion, this investigation has provided valuable insights and contributions to the cement industry, specifically in the field of combustion airflow and erosion mitigation. By collaborating with a cement plant Českomoravský cement, a.s., Mokrá facility, conducting detailed measurements, constructing a real-life burner model, and performing simulations, several important findings were obtained. The research helped in understanding the behaviour of combustion air inside the burner, optimizing the flow to achieve desired outcome parameters, and proposing several approaches to reduce erosive wear. These findings have the potential to enhance the operational efficiency and longevity of burners in the cement industry, ultimately leading to improved performance and cost savings.

Overall, performing a CFD analysis involves a significant amount of work that may not be immediately apparent. The images presented in the final version of the study represent the culmination of extensive behind-the-scenes efforts and the successful completion of the study.

This investigation serves as a contribution to the field, highlighting the importance of research and innovation in addressing industry-specific challenges and improving operational practices.

Nomenclature

a	Velocity of sound [m/s]
A_t	a total area of the tangential inlets, [m^2]
$C_{1\varepsilon}$,$C_{2\varepsilon}$	model constants, [-]
Cp	Specific heat capacity at constant pressure, [kJ/kg]
C_D	drag coefficient, [-]
Cv	constant representing the flow of liquid that will create a pressure drop of 1 bar, [m^3/h]
d	diameter [m]
d_0	nozzle diameter, [m]
D_I, D_{II}	Damkohler Number, [-]
E	mass of eroded material, [kg]
Eu	Euler Number, [-]
g	acceleration due to gravity, [m/s^2]
$\dot{G_0}$	nozzle flux of linear momentum, [kg·m/s]
G_k	generation of turbulence kinetic energy due to the mean velocity gradients, [m^2/s^2]
G_b	generation of turbulence kinetic energy due to buoyancy, [m^2/s^2]
K	factor relating to the shape of the velocity profile, [-]
k	thermal conductivity [W/mK] also a model constant, [-]
L	length, [m]
$\dot{L_0}$	nozzle flux of angular momentum, [kg·m^2/s]
M	Craya-Curtet parameter, [-] also Molar mass [kJ/kmol]
Ma	Mach Number, [-]
$\dot{m}$	mass flow rate, [kg/s]
P	static or gauge pressure, [Pa]
Pe	Peclet number [-]
Pr	Prandtl number, [-]
Q	net heat transfer, [W] also flow rate, [m^3N/h]
R	discharge ratio, [-] also Universal gas constant, [kJ/kmol·K]
Re	Reynolds number, [-]
r	radius, [m]

S swirl number, [-]

S_ε turbulence source

S_g geometrical swirl number, [-]

t temperature [°C] or time [s]

T temperature [K]

u velocity parallel to the bed surface, [m/s]

$\dot{V}$ flowrate, [m^3N/h]

V, v velocity of the impacting particle [m/s]

Y mass fraction, [-]

Greek

α_k inverse effective Prandtl numbers for k, [-]

α_ε inverse effective Prandtl numbers for ε, [-]

γ impact angle, [°]

δ* boundary layer displacement thickness defined as 1.74/√Re, [-]

ε Turbulence dissipation rate, [m^3/s^3]

λ conductivity (granular of thermal), [W/(m·K)]

ρ bulk density [kg/m^3]

ρ_{t20} air density at 20 °C, [kg/m^3]

τ time [s]

μ molecular viscosity, [Pa·s]

υ kinematic viscosity [m^2/s]

ω angular velocity [1/s]

Subscript

0 jet

1 velocity before the collision

2 velocity after the collision

a surrounding

e radius at which the tangential inlets of the swirl vanes are joined in relation to the centre axis

eff effective

n	normal direction to the wall
p	particle
sph	spherical-particle
T	total
τ	tangential

References

[1] BRZOBOHATÝ, Lukáš. Separation of raw meal transport air [online]. Brno, 2013. Available from: http://hdl.handle.net/11012/27898. Master thesis. Brno University of Technology. Faculty of Mechanical Engineering. Department of Process Engineering. Thesis supervisor Zdeněk Jegla.

[2] HENDRIKS, C A, WORRELL, E, PRICE, L, MARTIN, N, OZAWA MEIDA, L, de JAGER, D and RIEMER, P, 1999, Emission Reduction of Greenhouse Gases from the Cement Industry, Greenhouse Gas Control Technologies, Cairns, Australia

[3] VOLDSUND, Mari, GARDARSDOTTIR, Stefania Osk, DE LENA, Edoardo, PÉREZ-CALVO, José-Francisco, JAMALI, Armin, BERSTAD, David, FU, Chao, ROMANO, Matteo, ROUSSANALY, Simon, ANANTHARAMAN, Rahul, HOPPE, Helmut, SUTTER, Daniel, MAZZOTTI, Marco, GAZZANI, Matteo, CINTI, Giovanni and JORDAL, Kristin, 2019. Comparison of Technologies for CO2 Capture from Cement Production—Part 1: Technical Evaluation. *Energies*. January 2019. Vol. 12, no. 3, pp. 559. DOI 10.3390/en12030559.

[4] SCHORCHT, F., KOURTI, I., SCALET, B., ROUDIER, S., SANCHO, L. Best Available Techniques (BAT) Reference Document for the Production of Cement, Lime and Magnesium Oxide. 2013, DOI: 10.2788/12850

[5] HEIDELBERGCEMENT AG. (2019). How Cement Is Made. Brochure. Heidelberg Materials. Online. [Accessed 17 April 2023] Retrieved from: https://www.heidelbergmaterials.com/en/how-cement-is-made#:~:text=The%20most%20important%20raw%20materials,by%20ripping%20using%20heavy%20machinery.

[6] MATEUS, Maria Margarida, NEUPARTH, Teresa and CECÍLIO, Duarte Morais, 2023. Modern Kiln Burner Technology in the Current Energy Climate: Pushing the Limits of Alternative Fuel Substitution. *Fire*. February 2023. Vol. 6, no. 2, pp. 74. DOI 10.3390/fire6020074.

[7] Coal for Cement: Present and Future Trends; Global Cement: Epsom, UK, 2016

[8] O. LABAHN and B. KOHLHAAS, Cement Engineers' Handbook, 4th ed. Bauverlag GMBH, Wiesbaden, Germany, 1983.

[9] C. GRECO, G. PICCIOTTI, R. M. GRECO, and G. M. FERREIRA, "Fuel Selection and Use," in Innovations in Portland Cement Manufacturing, 1st ed., J. I. Bhatty, F. M. Miller, S. H. Kosmatka, and R. P. Bohan, Eds. Skokie, Illinois, USA: Portland Cement Association, 2011, pp. 239–308.

[10] CHINYAMA, Moses P. M., 2011. Alternative Fuels in Cement Manufacturing. In: *Alternative Fuel*. Online. IntechOpen. [Accessed 4 May 2023]. ISBN 978-953-307-372-9.

[11] L. K. NØRSKOV (2012), "Combustion of Solid Alternative Fuels in the Cement Kiln Burner," Ph.D. Thesis, Technical University of Denmark.

[12] PEDERSEN, M. N. (2018). “Co-firing of Alternative Fuels in Cement Kiln Burners”. Technical University of Denmark.

[13] Unitherm Cemcon *www.unitherm.co.at*, 2022

[14] M. H. VACCARO, “Low NOx rotary kiln burner technology: design principles & case study,” in 2002 IEEE Cement Industry Technical Conference, 2002, pp. 265–270.

[15] Reinhard, RINGDORFER, “Evolution through experience,” *World of cement*. February 2016.

[16] RICCI, Louis and PIVER, Gaël Le, 2017. Burner with adjustable air or gas injection Online. EP3177872A1. 14 June 2017. [Accessed 4 December 2022]. Retrieved from: https://patents.google.com/patent/EP3177872A1/en

[17] R. H. NOBIS, “Latest rotary kiln burner technology: Possibilities and experiences,” IEEE Transactions on Industry Applications, vol. 27, no. 5, pp. 798–806, 1991.

[18] N. RAJARATNAM, Turbulent Jets. Amsterdam: Elsevier, 1976.

[19] A. A. BOATENG, Rotary Kilns Transport Phenomena and Transport Process, 1st ed. Oxford, UK: Butterworth-Heinemann, 2008.

[20] NGADI, Z and LAHLAOUTI, M L, 2017. *CFD modeling of the gas–particle flow behaviour in kiln burner pipe*. 2017.

[21] MA, Ai-chun, ZHOU, Jie-min, OU, Jian-ping and LI, Wang-xing, 2006. CFD prediction of physical field for multi-air channel pulverized coal burner in rotary kiln. *Journal of Central South University of Technology*. February 2006. Vol. 13, no. 1, pp. 75–79. DOI 10.1007/s11771-006-0110-9.

[22] S. WANG, J. LU, W. LI, J. LI, and Z. HU. “Modeling of pulverized coal combustion in cement rotary kiln,” Energy & Fuels, 20, 2350–2356, 2006.

[23] BHAD, T.P .SARKAR, S. KAUSHIK, A. HERWADKAR, *CFD modeling of a cement kiln with multi channel burner for optimization of flame profile*, the Seventh International Conference on CFD in the Minerals and Process Industries, Australia, 2009.

[24] NGADI, Z. and LAHLAOUTI, M. L., 2021. CFD modeling of petcoke co-combustion in a real cement kiln: The effect of the turbulence-chemistry interaction model applied with K-ϵ variations. *International Review of Applied Sciences and Engineering*. 27 September 2021. Vol. 13, no. 2, pp. 148–163. DOI 10.1556/1848.2021.00326.

[25] WILCOX, D.C. Turbulence Modeling for CFD. 3rd. S.l.: Dcw Industries, Incorporated, 2006. ISBN 1928729088.

[26] MENTER, F. R., LECHNER, R., MATYUSHENKO, A.: Best Practice: RANS Turbulence Modeling in Ansys CFD. ANSYS, Inc., Canonsburg, PA, USA, 2022.

[27] HIROMI ARIYARATNE, W. K. W. K., MALAGALAGE, Anjana, MELAAEN, Morten C. and ANDRÉ TOKHEIM, Lars, 2014. CFD Modeling of Meat and Bone Meal Combustion in a Rotary Cement Kiln. *International Journal of Modeling and Optimization*. August 2014. Vol. 4, no. 4, pp. 263–272. DOI 10.7763/IJMO.2014.V4.384.

[28] ANSYS FLUENT 12.0 Theory Guide. Online. [Accessed 28 February 2023]. Retrieved from: https://www.afs.enea.it/project/neptunius/docs/fluent/html/th/main_pre.htm

[29] ZAHARI, Nazirul, HAFIZ, Mohd, MOHD SIDEK, Lariyah, MOHAMAD, Daud, ITAM, Zarina, RAMLI, Muhammad, SYAMSIR, Agusril, ABAS, Aizat and RASHID, M., 2018. Introduction of discrete phase model (DPM) in fluid flow: A review. In: *AIP Conference Proceedings*. 12 November 2018. pp. 020234. DOI 10.1063/1.5066875.

[30] MORSI, S. A. and ALEXANDER, A. J., 1972. An investigation of particle trajectories in two-phase flow systems. Journal of Fluid Mechanics. September 1972. Vol. 55, no. 2, pp. 193–208. DOI 10.1017/S0022112072001806.

[31] HAIDER, A. and LEVENSPIEL, O., 1989. Drag coefficient and terminal velocity of spherical and nonspherical particles. Powder Technology. 1 May 1989. Vol. 58, no. 1, pp. 63–70. DOI 10.1016/0032-5910(89)80008-7.

[32] ANSYS FLUENT 12.0 User's Guide. Online. [Accessed 15 March 2023]. Retrieved from: https://www.afs.enea.it/project/neptunius/docs/fluent/html/ug/main_pre.htm

[33] BERMÚDEZ, A., FERRÍN, J.L., LIÑÁN, A. and SAAVEDRA, L., 2011. Numerical simulation of group combustion of pulverized coal. *Combustion and Flame*. September 2011. Vol. 158, no. 9, pp. 1852–1865. DOI 10.1016/j.combustflame.2011.02.002.

[34] BAŠTA, Jiří. Hydraulika a řízení otopných soustav. Praha: Vydavatelství ČVUT, 2003. ISBN 80-01-02808-9.

[35] HERNIK, B. Numerical Study of the Erosion Process and Transport of Pulverized Coal–Air Mixture in the Mill-Duct System. Energies 2022, 15, 899. https://doi.org/10.3390/en15030899

[36] OGUNLELA, Paul T., GIDDINGS, Donald, BENNETT, Chris, BORN, Stefan, KLAASSEN, Margot, GENNISSEN, Isaac and FARNISH, Richard, 2022. CFD Approach to the Influence of Particle Size on Erosive Wear in Coal Riser Pipes. *Journal of Fluid Flow, Heat and Mass Transfer (JFFHMT)*. 6 June 2022. Vol. 9, no. 1, pp. 43–48.

[37] HERNIK, B.; PRONOBIS, M.; WEJKOWSKI, R.; WOJNAR, W. Experimental verification of a CFD model intended for the determination of restitution coefficients used in erosion modelling. E3S Web Conf. 2017, 13, 05001

[38] ZHANG, Zhigang, LAN, Xiangyun, WEN, Guangcai, LONG, Qingming and YANG, Xuelin, 2021. An Experimental Study on the Particle Size and Shape Distribution of Coal Drill Cuttings by Dynamic Image Analysis. *Geofluids*. 21 August 2021. Vol. 2021, pp. e5588248. DOI 10.1155/2021/5588248.

[39] VONDÁL, Jiří. Computational Modeling of Turbulent Swirling Diffusion Flames [online]. Brno, 2012 [cit. 2023-05-26]. Available: http://hdl.handle.net/11012/10127. Doctoral thesis. Brno University of Technology, Faculty of Mechanical Engineering, Institute of Process Engineering. Thesis supervisor Jiří Hájek.